

Study of the $e^+e^- \rightarrow \pi^+\pi^-\omega$ process at center-of-mass energies between 4.0 and 4.6 GeV

The BESIII collaboration



ABSTRACT: Using 15.6 fb^{-1} of e^+e^- collision data collected at twenty-four center-of-mass energies from 4.0 to 4.6 GeV with the BESIII detector, the helicity amplitudes of the process $e^+e^- \rightarrow \pi^+\pi^-\omega$ are analyzed for the first time. Born cross section measurements of two-body intermediate resonance states with statistical significance greater than 5σ are presented, such as $f_0(500)$, $f_0(980)$, $f_2(1270)$, $f_0(1370)$, $b_1(1235)^\pm$, and $\rho(1450)^\pm$. In addition, evidence of a resonance state in $e^+e^- \rightarrow \pi^+\pi^-\omega$ production is found. The mass of this state obtained by line shape fitting is about $4.2 \text{ GeV}/c^2$, which is consistent with the production of $\psi(4160)$ or $Y(4220)$.

KEYWORDS: Charmonium (-like), Born cross section measurement, helicity amplitude analysis

Contents

1	INTRODUCTION	1
2	BESIII DETECTOR AND MONTE CARLO SIMULATION	2
3	EVENT SELECTION AND BACKGROUND ANALYSIS	3
4	AMPLITUDE ANALYSIS	4
4.1	Kinematic variable and helicity angles	4
4.2	Decay amplitude	5
4.3	Simultaneous fit	8
4.4	Intermediate states in $\pi^+\pi^-\omega$ final state	9
4.5	Fit results	10
5	BORN CROSS SECTION	12
5.1	ISR correction factor	12
5.2	Born cross section of $e^+e^- \rightarrow \pi^+\pi^-\omega$	13
5.3	Born cross section for intermediate states	13
6	SYSTEMATIC UNCERTAINTY	13
6.1	Uncertainty of the Born cross section	13
6.2	Uncertainty of the Born cross section for intermediate process	17
7	FIT TO THE LINE SHAPE	17
8	SUMMARY	20

1 INTRODUCTION

In recent years the study of charmonium-like(XYZ) states has become a hot topic for both experimental and theoretical physics due to their unexpected resonance parameters and exotic decay patterns [1]. Since 2003, a series of charmonium-like states inconsistent with the quark model, such as the $X(3872)$ [2], $Y(4260)$ [3] and $Z_c(3900)$ [4, 5], have been observed. In particular, the vector charmonium-like state $Y(4260)$ was observed by the BaBar experiment in $e^+e^- \rightarrow \gamma_{\text{ISR}}\pi^+\pi^-J/\psi$ [3] and was confirmed by the CLEO and Belle experiments [6, 7]. In 2017, the BESIII experiment performed a dedicated scan of $e^+e^- \rightarrow \pi^+\pi^-J/\psi$ and observed two structures in this energy region. The one with the mass $M = (4222.0 \pm 3.1 \pm 1.4) \text{ MeV}/c^2$ [8] was regarded as the previously observed $Y(4260)$, and renamed as $Y(4220)$. The $Y(4220)$ was then confirmed in the Born cross section line shapes of $e^+e^- \rightarrow \omega\chi_{c0}$ [9], $\pi^+\pi^-h_c$ [10], $\pi^+\pi^-\psi(3686)$ [11], and $\pi^+D^0D^{*-}$ [12] measured

by the BESIII experiment. The other structure was identified with the $Y(4360)$, which was previously observed in $e^+e^- \rightarrow \gamma_{\text{ISR}}\pi^+\pi^-\psi(3686)$ by the BaBar experiment in 2007 [13]. Theoretically, many assignments, such as a tetraquark state [15–22], a hybrid state [23–27], a hadro-charmonium state [28–31], a molecular state [32–35], a kinematic effect [36–39], a baryonium state [40], etc., were proposed to explain the Y state.

The traditional charmonium states, such as $\psi(4160)$ and $\psi(4040)$, were observed in $e^+e^- \rightarrow$ hadrons [41–43] and $B^+ \rightarrow K^+\mu^+\mu^-$ [44]. However, their decays into light hadron final states have never been observed. Many searches have been performed for these charmonium(-like) states produced in e^+e^- collisions and decaying to light hadron final states, including $K_S^0 K^\pm \pi^\mp \pi^0 / \eta$ [45], $K_S^0 K^\pm \pi^\mp$ [46], $2(p\bar{p})$ [47], and $\pi^+\pi^-\pi^+\pi^-\pi^0$ [48]. Only evidence for $\psi(4040) \rightarrow \pi^+\pi^-\pi^+\pi^-\pi^0$ has been reported.

In this paper, we measure the Born cross sections of $e^+e^- \rightarrow \pi^+\pi^-\omega$ at 24 center-of-mass (c.m.) energies between 4.0 and 4.6 GeV, to search for the charmonium(-like) states decaying into light hadron final states. Furthermore, we study intermediate states in the $e^+e^- \rightarrow \pi^+\pi^-\omega$ process via partial wave analysis (PWA).

2 BESIII DETECTOR AND MONTE CARLO SIMULATION

The BESIII detector is a magnetic spectrometer [50] located at the Beijing Electron Positron Collider (BEPCII) [51]. The cylindrical core of the BESIII detector consists of a helium-based multilayer drift chamber (MDC), a plastic scintillator time-of-flight system (TOF), and a CsI(Tl) electromagnetic calorimeter (EMC), which are all enclosed in a superconducting solenoidal magnet providing a 1.0 T magnetic field [52]. The solenoid is supported by an octagonal flux-return yoke with resistive plate counter muon identifier modules interleaved with steel. The acceptance of charged particles and photons is 93% over 4π solid angle. The charged-particle momentum resolution at 1 GeV/ c is 0.5%, and the specific ionization energy loss (dE/dx) resolution is 6% for the electrons from Bhabha scattering. The EMC measures photon energies with a resolution of 2.5% (5%) at 1 GeV in the barrel (end cap) region. The time resolution of the TOF barrel part is 68 ps, while that of the end cap part is 110 ps. The end cap TOF system was upgraded in 2015 with multi-gap resistive plate chamber technology, providing a time resolution of 60 ps [53]; about 84% of the data used here benefits from this improvement.

This analysis uses data sets taken at twenty-four c.m. energies ranging from 4.0 to 4.6 GeV. For each data set, the c.m. energy is calibrated by the di-muon process $e^+e^- \rightarrow (\gamma_{\text{ISR,FSR}})\mu^+\mu^-$ [54], where $\gamma_{\text{ISR,FSR}}$ stands for possible initial state radiative (ISR) or final state radiative (FSR) photons. The integrated luminosity (\mathcal{L}_{int}) is determined using large-angle Bhabha events [55], and the total integrated luminosity of all data sets is 15.6 fb $^{-1}$.

The BESIII detector is modeled with a Monte Carlo (MC) simulation using the software framework BOOST [56], based on GEANT4 [57], which includes the geometric and material description of the BESIII detector [58, 59], the detector response, and digitization models, as well as the detector running conditions and performances. Simulated MC samples generated by a phase space (PHSP) model with KKMC [60] are used for efficiency corrections in the

PWA, and the TOY MC samples with detector simulation generated by ConExc [61] are used to determine detection efficiencies used for the Born cross-section determinations. The TOY MC events are generated based on helicity amplitude model with parameters fixed to the PWA results. The inclusive MC sample generated at $\sqrt{s} = 4.178$ GeV with KKMC [60] is used to study the potential backgrounds.

3 EVENT SELECTION AND BACKGROUND ANALYSIS

For $e^+e^- \rightarrow \pi^+\pi^-\omega$, $\omega \rightarrow \pi^+\pi^-\pi^0$, $\pi^0 \rightarrow \gamma\gamma$, the final state is characterized by four charged pion tracks and two photons. For each charged track, the distance of closest approach to the interaction point is required to be within 10 cm in the beam direction and within 1 cm in the plane perpendicular to the beam direction. The track polar angle (θ) must be within the fiducial volume of the MDC, *i.e.*, $|\cos\theta| < 0.93$. Particle identification (PID) for charged tracks combines the dE/dx and TOF information to form likelihoods $\mathcal{L}(h)$ ($h = p, K, \pi$) for each particle hypothesis. Momentum-dependent PID is used to improve detection efficiency. Charged tracks with momentum less than 0.9 GeV/ c , are identified as pion candidates if their likelihoods satisfy $\mathcal{L}(\pi) > \mathcal{L}(K)$ and $\mathcal{L}(\pi) > \mathcal{L}(p)$. Those with momentum greater than 0.9 GeV/ c are assigned as pion candidates with no PID requirement.

Isolated EMC showers are considered as photon candidates. The deposited energy of each shower must be above 25 MeV in the barrel region ($|\cos\theta| < 0.80$) and 50 MeV in the end cap region ($0.86 < |\cos\theta| < 0.92$). Showers are required to occur within 700 ns of the event start time to suppress noise. Photon pairs with an invariant mass in the interval $0.11 \sim 0.15$ GeV/ c^2 are taken as π^0 candidates.

To reduce potential peaking backgrounds from $e^+e^- \rightarrow \gamma\omega$ with γ converting to e^+e^- , the E_{EMC}/p of the pion candidate from non- ω decay is required to be less than 0.9, where p and E_{EMC} are momentum and EMC energy deposit associated with the track, respectively. To suppress the backgrounds from $e^+e^- \rightarrow K_S^0\pi^+\pi^-\pi^0$ and $e^+e^- \rightarrow \chi_{c0}\omega$ [62], the invariant mass of all four $\pi^+\pi^-$ combinations are required to be outside the range of (0.49, 0.51) and (3.39, 3.44) GeV/ c^2 , respectively. To further suppress the background and improve the mass resolution, we perform a five-constraint (5C) kinematic fit to the known initial four-momentum and π^0 mass [1]. The χ_{5C}^2 under the hypothesis of $e^+e^- \rightarrow \pi^+\pi^-\pi^+\pi^-\pi^0$ with $\pi^0 \rightarrow \gamma\gamma$ is required to be less than 60. If more than one combination satisfies the above selection requirements, only the one with the smallest χ_{5C}^2 is kept. To suppress background contribution from the final states with an additional photon, the χ_{5C}^2 under the $\pi^+\pi^-\pi^+\pi^-\pi^0$ hypothesis is required to be less than that under the $\pi^+\pi^-\pi^+\pi^-\pi^0\gamma$ hypothesis: $\chi_{5C}^2(\pi^+\pi^-\pi^+\pi^-\pi^0) < \chi_{5C}^2(\pi^+\pi^-\pi^+\pi^-\pi^0\gamma)$.

In each event, there are four $\pi^+\pi^-\pi^0$ combinations; the one with the invariant mass $M_{\pi^+\pi^-\pi^0}$ closest to the known ω mass [1] is chosen as the ω candidate. This may distort the combinatoric background shape. A study of an $e^+e^- \rightarrow \pi^+\pi^-\pi^+\pi^-\pi^0$ MC sample leads to a smooth distribution of the invariant mass of combinatoric $\pi^+\pi^-\pi^0$ that can be described by a polynomial function. A study based on the signal MC sample shows that the ratio of the yield of combinatoric $\pi^+\pi^-\pi^0$ background to the signal yield is 1.4%

and results in a negligible difference of 0.1% on the fitted signal yield. Figure 1 shows the $M_{\pi^+\pi^-\pi^0}$ distribution of the accepted events from the data sample taken at $\sqrt{s} = 4.178$ GeV. To extract the number of signal events, an unbinned extended maximum-likelihood fit is performed on the $M_{\pi^+\pi^-\pi^0}$ distribution. The signal shape is a MC-derived shape convolved with an additional Gaussian smearing function, and the background shape is a second-order Chebychev polynomial function. The signal yields are listed in Table 3. Based on the $M_{\pi^+\pi^-\pi^0}$ resolution from fitting, the ω signal region is defined as $M_{\pi^+\pi^-\pi^0} \in (0.76, 0.82)$ GeV/ c^2 , while the ω sideband regions are defined as the regions $M_{\pi^+\pi^-\pi^0} \in (0.68, 0.74)$ GeV/ c^2 and $M_{\pi^+\pi^-\pi^0} \in (0.84, 0.90)$ GeV/ c^2 .

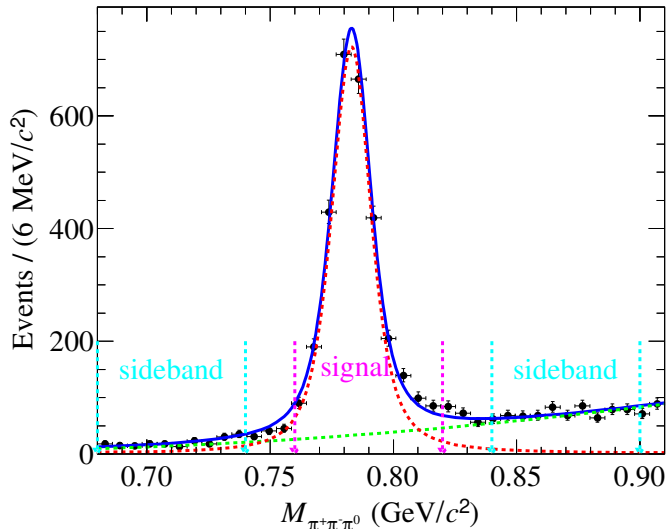


Figure 1. Distribution of $M_{\pi^+\pi^-\pi^0}$ for events selected at $\sqrt{s} = 4.1780$ GeV (black points with error bars). The blue solid curve is the total fit result, the red dashed curve is the fitted signal shape and the green dashed curve is the fitted background shape. The region between two dashed pink arrows is the ω signal region, while the regions between the pairs of neighboring dashed blue arrows are the ω sideband regions.

4 AMPLITUDE ANALYSIS

4.1 Kinematic variable and helicity angles

The $\pi^+\pi^-\omega$ final state is produced from the e^+e^- annihilation into a virtual photon, followed by hadronization into the $\pi^+(p_1)\pi^-(p_2)\omega(p_3)$ final state, where p_i ($i = 1, 2, 3$) denote particle momenta after the kinematic fit. The $\pi^+\pi^-\omega$ final state may be produced non-resonantly, or via an intermediate resonance and subsequent decay; the possible resonance diagrams are shown in Fig. 2.

The amplitudes for these diagrams are constructed using the helicity formalism. Taking the first diagram in Fig. 2 as an example, one may define the helicity rotation angles as in

Fig. 3. For resonance R_1 the polar angle ($\theta_{[12]}^{[123]}$) is defined as the angle spanned between the R_1 momentum and the positron beam direction, the azimuthal angle ($\phi_{[12]}^{[123]}$) is the angle between the R_1 production plane formed by the R_1 momentum and the z axis and the plane formed by the x and z axes. Here, xyz denotes the laboratory coordinates. The helicity amplitude for $\gamma^* \rightarrow R_1(\lambda_R)\omega(\lambda_3)$ is denoted by $F_{\lambda_R,\lambda_3}^{\gamma^*}$ with specified helicity λ_R and λ_3 . For the $R_1 \rightarrow \pi^+\pi^-$ decay, the azimuthal angle ($\phi_{[1]}^{[12]}$) is defined as the angle between the R_1 production plane and its decay plane, formed by the momenta of $\pi^+\pi^-$ from R_1 . After boosting the two pion momenta to the R_1 rest frame, they are still located in the same decay plane. The polar angle ($\theta_{[1]}^{[12]}$) for π^+ is defined as the angle between the π^+ and R_1 momenta in the R_1 rest frame. The helicity amplitude of this decay is denoted by $F_{0,0}^{R_1}$. Helicity angles for the processes (b) and (c) are defined analogously. Table 1 summarizes the helicity angles and amplitudes for the three processes.

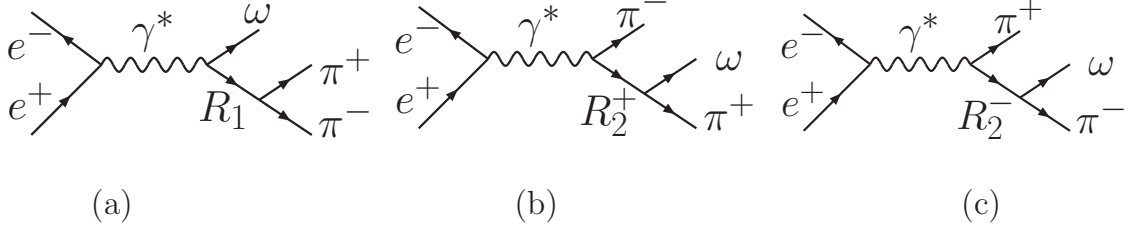


Figure 2. The Feynman diagrams of quasi-two body decays in the process $e^+e^- \rightarrow \pi^+\pi^-\omega$ with different subprocesses: (a) $e^+e^- \rightarrow R_1\omega$, $R_1 \rightarrow \pi^+\pi^-$; (b) $e^+e^- \rightarrow \pi^-R_2^+$, $R_2^+ \rightarrow \pi^+\omega$; and (c) $e^+e^- \rightarrow \pi^+R_2^-$, $R_2^- \rightarrow \pi^-\omega$, where R_1 and R_2^\pm denote intermediate states.

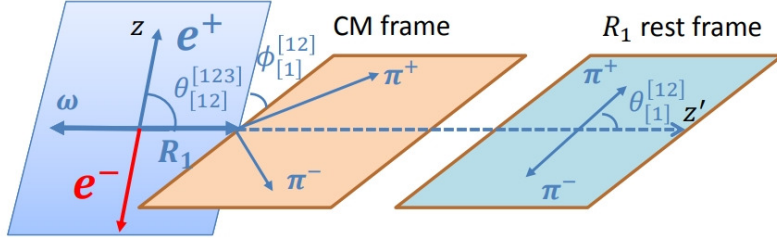


Figure 3. Definitions of helicity rotation angles for the process $e^+e^- \rightarrow R_1\omega$, $R_1 \rightarrow \pi^+\pi^-$.

4.2 Decay amplitude

The decay amplitude for the process (a) is

$$A_1(m, \lambda_3) = \sum_{\lambda_R} F_{\lambda_R,\lambda_3}^{\gamma^*} D_{m,\lambda_R-\lambda_3}^{1*}(\phi_{[12]}^{[123]}, \theta_{[12]}^{[123]}, 0) BW(m_{12}) F_{0,0}^{R_1} D_{\lambda_R,0}^{J*}(\phi_{[1]}^{[12]}, \theta_{[1]}^{[12]}, 0), \quad (4.1)$$

where $D_{m,\lambda}^J(\phi, \theta, 0)$ is the Wigner D -function, J is the spin quantum number of resonance R_1 , and BW denotes the Breit-Wigner function.

Table 1. Variable definitions for the helicity angles and helicity amplitudes of the sequential processes (a), (b) and (c) shown in Fig. 2. The λ_i denotes the helicity value for the corresponding particle, and m denotes the spin z projection of virtual photon (γ^*) in electron-positron annihilation.

Process	Helicity angle	Helicity amplitude
$e^+e^- \rightarrow \gamma^*(m) \rightarrow R_1(\lambda_R)\omega(\lambda_3)$	$\theta_{[12]}^{[123]}, \phi_{[12]}^{[123]}$	$F_{\lambda_R, \lambda_3}^{\gamma^*}$
$R_1 \rightarrow \pi^+\pi^-$	$\theta_{[1]}^{[12]}, \phi_{[1]}^{[12]}$	$F_{0,0}^{R_1}$
$e^+e^- \rightarrow \gamma^*(m) \rightarrow R_2^+(\lambda_+)\pi^-$	$\theta_{[13]}^{[123]}, \phi_{[13]}^{[123]}$	$F_{\lambda_+, 0}^{\gamma^*}$
$R_2^+ \rightarrow \omega(\lambda'_3)\pi^+$	$\theta_{[3]}^{[13]}, \phi_{[3]}^{[13]}$	$F_{\lambda'_3, 0}^{R_2^+}$
$e^+e^- \rightarrow \gamma^*(m) \rightarrow R_2^-(\lambda_-)\pi^+$	$\theta_{[23]}^{[123]}, \phi_{[23]}^{[123]}$	$F_{\lambda_-, 0}^{\gamma^*}$
$R_2^- \rightarrow \omega(\lambda''_3)\pi^-$	$\theta_{[3]}^{[23]}, \phi_{[3]}^{[23]}$	$F_{\lambda''_3, 0}^{R_2^-}$

The decay amplitude for the process (b) is

$$\begin{aligned}
A_2(m, \lambda_3) = & \sum_{\lambda_+, \lambda'_3} F_{\lambda_+, 0}^{\gamma^*} D_{m, \lambda_+}^{1*}(\phi_{[13]}^{[123]}, \theta_{[13]}^{[123]}, 0) BW(m_{13}) F_{\lambda'_3, 0}^{R_2^+} D_{\lambda_+, \lambda'_3}^{J*}(\phi_{[3]}^{[13]}, \theta_{[3]}^{[13]}, 0) \\
& \times D_{\lambda'_3, \lambda_3}^1(\phi'_3, \theta'_3, 0),
\end{aligned} \tag{4.2}$$

where J is the spin of R_2^+ . Since the ω helicity defined in the R_2^+ helicity system is different from that defined in the process (a), one needs to perform a rotation by the angles (θ'_3, ϕ'_3) to align the ω helicity to coincide with that in the process (a). This issue has been addressed in the analyses [63, 64] and derived in detail in Ref. [65].

The decay amplitude for the process (c) reads

$$\begin{aligned}
A_3(m, \lambda_3) = & \sum_{\lambda_-, \lambda''_3} F_{\lambda_-, 0}^{\gamma^*} D_{m, \lambda_-}^{1*}(\phi_{[23]}^{[123]}, \theta_{[23]}^{[123]}, 0) BW(m_{23}) F_{\lambda''_3, 0}^{R_2^-} D_{\lambda_-, \lambda''_3}^{J*}(\phi_{[3]}^{[23]}, \theta_{[3]}^{[23]}, 0) \\
& \times D_{\lambda''_3, \lambda_3}^1(\phi''_3, \theta''_3, 0),
\end{aligned} \tag{4.3}$$

where the Wigner $D_{\lambda''_3, \lambda_3}^1(\phi''_3, \theta''_3, 0)$ function is used to align the ω helicity to coincide with that defined in the process (a).

For the direct three-body process $e^+e^- \rightarrow \pi^+\pi^-\omega$, the helicity amplitude is written as [66]:

$$A_4(m, \lambda_3) = \sum_{\mu} F_{\mu, \lambda_3} D_{m, \mu}^{1*}(\alpha, \beta, \gamma), \tag{4.4}$$

where μ is the z component of the spin J of the virtual photon in the helicity system, and $m(\lambda_3)$ is the helicity value for $\gamma^*(\omega)$. Here, α , β , and γ are the Euler angles as defined in [66] (see Fig. 4). F_{μ, λ_3} is the helicity amplitude; parity conservation requires $F_{\pm, \lambda_3} = -F_{\pm, -\lambda_3}$ and $F_{0, \lambda_3} = F_{0, -\lambda_3}$. Parity conservation also requires $F_{\pm, \lambda_3}(E_i) = -F_{\pm, -\lambda_3}(E_i)$ and $F_{0, \lambda_3}(E_i) = F_{0, -\lambda_3}(E_i)$, where $E_i (i = 1, 2, 3)$ corresponds to the energy of the final state $\pi^+\pi^-\omega$.

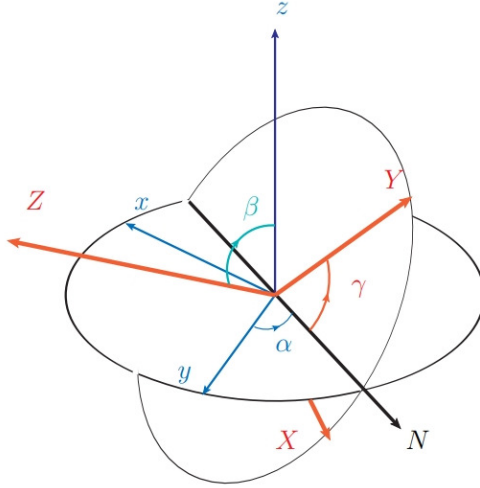


Figure 4. The illustration of rotations to carry the ω , π^+ and π^- orientations from the rest frame xyz to the three-body helicity system XYZ by the three Euler angles α , β and γ .

One usually expands the helicity amplitudes in terms of the partial waves for the two-body decay in the LS -coupling scheme [66]. For a spin- J particle decay $J \rightarrow s + \sigma$, it follows

$$F_{\lambda,\nu}^J = \sum_{ls} \left(\frac{2l+1}{2J+1} \right)^{1/2} \langle l0S\delta | J\delta \rangle \langle s\lambda\sigma - \nu | S\delta \rangle g_{lS} r^l \frac{B_l(r)}{B_l(r_0)}, \quad (4.5)$$

where λ and ν are the helicities of two final-state particles s and σ with $\delta = \lambda - \nu$, and g_{lS} is a coupling constant, S is the total spin $\mathbf{S} = \mathbf{s} + \sigma$, l is the orbital angular momentum, $r = |\mathbf{r}|$, where \mathbf{r} is the relative momentum between the two daughter particles in their mother rest frame, r_0 corresponds to the value at the resonance's known mass. $B_l(r)$ is the Blatt-Weisskopf factor [66], which suppresses the contributions with higher angular momentum. The Blatt-Weisskopf factors up to $l = 4$ are

$$\begin{aligned} B_0(r)/B_0(r_0) &= 1, \\ B_1(r)/B_1(r_0) &= \frac{\sqrt{1+(dr_0)^2}}{\sqrt{1+(dr)^2}}, \\ B_2(r)/B_2(r_0) &= \frac{\sqrt{9+3(dr_0)^2+(dr_0)^4}}{\sqrt{9+3(dr)^2+(dr)^4}}, \\ B_3(r)/B_3(r_0) &= \frac{\sqrt{225+45(dr_0)^2+6(dr_0)^4+(dr_0)^6}}{\sqrt{225+45(dr)^2+6(dr)^4+(dr)^6}}, \\ B_4(r)/B_4(r_0) &= \frac{\sqrt{11025+1575(dr_0)^2+135(dr_0)^4+10(dr_0)^6+(dr_0)^8}}{\sqrt{11025+1575(dr)^2+135(dr)^4+10(dr)^6+(dr)^8}}, \end{aligned} \quad (4.6)$$

where d is a constant fixed to 3 GeV^{-1} for the meson final states [63].

The differential cross section is given by

$$d\sigma = \frac{1}{2} \sum_{m, \lambda_3} \Omega(\lambda_3) \left| \sum_{j=1}^4 A_j(m, \lambda_3) \right|^2 d\Phi, \quad (4.7)$$

where $m = \pm 1$ due to the polarization of the virtual photon being produced from e^+e^- annihilation, and $d\Phi$ is the element of standard three-body PHSP. The $\Omega(\lambda_3) = |\boldsymbol{\varepsilon}(\lambda_3) \cdot (\mathbf{q}_1 \times \mathbf{q}_2)|^2$ is the ω decay matrix element into the $\pi^+\pi^-\pi^0$ final states, where $\boldsymbol{\varepsilon}$ is the ω polarization vector, and $\mathbf{q}_1(\mathbf{q}_2)$ is the momentum vector for $\pi^+(\pi^-)$ from the ω decay. Here we factor out the *BW* function describing the ω line shape into the MC integration when applying the amplitude analysis to the data events.

4.3 Simultaneous fit

The relative magnitudes and phases of the coupling constants are determined by an unbinned maximum likelihood fit. The joint probability density function (PDF) for the events observed in the data sample is defined as

$$\mathcal{L} = \prod_{i=1}^N P_i(p_1, p_2, p_3, p_4, p_5), \quad (4.8)$$

where p_i ($i = 1, 2, \dots, 5$) denotes the four-vector momenta of the final state particles, and P_i is a probability to produce the i -th event. The normalized P_i is calculated from the differential cross section

$$P_i = \frac{(d\sigma/d\Phi)_i}{\sigma_{\text{MC}}}, \quad (4.9)$$

where σ_{MC} is the normalization factor which is calculated with a large MC sample as

$$\sigma_{\text{MC}} \approx \frac{1}{N_{\text{MC}}} \sum_{i=1}^{N_{\text{MC}}} \left(\frac{d\sigma}{d\Phi} \right)_i, \quad (4.10)$$

where N_{MC} is the number of events retained with the same selection criteria as for data sample.

For technical reasons, rather than maximizing \mathcal{L} , $S = -\ln \mathcal{L}$ is minimized using the package MINUIT [67]. To subtract the contribution of background, the $\ln \mathcal{L}$ function is replaced with

$$\ln \mathcal{L} = \ln \mathcal{L}_{\text{data}} - \ln \mathcal{L}_{\text{bkg}}, \quad (4.11)$$

where $\mathcal{L}_{\text{data}}$ and \mathcal{L}_{bkg} are the joint PDFs for data and background, respectively. The background events are obtained from the ω sideband regions mentioned in Section 3.

A simultaneous fit is performed to data sets collected at different c.m. energies. The common parameters for different data samples in this fit are the masses, widths, and Flatté parameters for the resonances. The total function is taken as the sum of individual ones, *i.e.*,

$$S' = - \sum_{j=1}^M \ln \mathcal{L}_j. \quad (4.12)$$

The signal yield for the i -th resonance, N_i , can be estimated by scaling its cross section ratio R_i to the number of net events

$$N_i = R_i(N_{\text{obs}} - N_{\text{bkg}}), \text{ with } R_i = \frac{\sigma_i}{\sigma_{\text{tot}}}, \quad (4.13)$$

where σ_i is the cross section for the i -th resonance as defined in Eq.(4.7), σ_{tot} is the total cross section, and N_{obs} and N_{bkg} are the numbers of observed events and background events, respectively. In the simultaneous fit, the background events are taken from the ω sideband regions, and the number N_{bkg} is estimated with the background PDF with the ω signal region (see Fig. 1).

The statistical uncertainty, ΔN_i , associated with the signal yield N_i , is estimated according to the error propagation formula using the covariance matrix, V , obtained in the simultaneous fit, *i.e.*

$$\Delta N_i^2 = \sum_{m=1}^{N_{\text{pars}}} \sum_{n=1}^{N_{\text{pars}}} \left(\frac{\partial N_i}{\partial X_m} \frac{\partial N_i}{\partial X_n} \right)_{\mathbf{X}=\boldsymbol{\mu}} V_{mn}(\mathbf{X}), \quad (4.14)$$

where \mathbf{X} is a vector containing parameters, and $\boldsymbol{\mu}$ contains the fitted values for all parameters. The sum runs over all N_{pars} parameters.

4.4 Intermediate states in $\pi^+\pi^-\omega$ final state

In the $\pi^+\pi^-$ and $\omega\pi^\pm$ mass spectrum, the $f_0(500)$, $f_0(980)$, $f_2(1270)$, $f_0(1370)$, $b_1(1235)^\pm$, $\rho(1450)^\pm$, and $\rho(1570)^\pm$ resonances are included in the amplitude model. The $f_0(980)$ line shape is parameterized by the Flatté formula:

$$BW_1(s) = \frac{1}{s - M^2 + i(g_1\rho_{\pi\pi}(s) + g_2\rho_{K\bar{K}}(s))}, \quad (4.15)$$

where $\rho(s) = 2k/\sqrt{s}$ and k is the momentum of the π or K in the resonance rest frame, g_1 and g_2/g_1 are fixed to the measured values (0.138 ± 0.010) GeV^2 and 4.45 ± 0.25 [68, 69], respectively. M is the mass of $f_0(980)$ taken from the PDG [1].

For the BW_2 function of a wide resonance, *e.g.*, $f_0(500)$, there are many parametrizations for the energy-dependent width [68, 69], and we take the one used by the E791 Collaboration in the nominal fit,

$$BW_2(s) = \frac{1}{s - m_0^2 + i\sqrt{s}\Gamma}, \text{ with } \Gamma = \sqrt{1 - \frac{4m_\pi^2}{s}}\Gamma_0, \quad (4.16)$$

where m_0 is the nominal mass of the resonance, and Γ_0 is its width. For other resonances, such as $b_1(1235)^\pm$, $f_0(1370)$, $f_2(1270)$, $\rho(1450)^\pm$, $\rho(1570)^\pm$, their line shapes are described with the BW_3 function,

$$BW_3(s) = \frac{1}{s - m_0^2 + i\sqrt{s}\Gamma}, \quad (4.17)$$

where the widths are fixed to the individual PDG values [1].

Based on the signal events in the $\pi^+\pi^-\pi^0$ mass spectrum, we select twelve c.m. energy points with relatively large statistics. We divide these selected points into two groups.

Group A includes the data sets taken at $\sqrt{s} = 4.0076, 4.1780, 4.1890, 4.1990, 4.2093,$ and 4.2188 GeV, and group B includes $\sqrt{s} = 4.2263, 4.2358, 4.2439, 4.2580, 4.2668,$ and 4.4156 GeV. To check the significance of each resonance and determine the nominal solution, a simultaneous fit is performed to the data from a given group. In each group, the cross sections of these intermediate states are regarded to be energy-dependent, so the parameters responsible for the virtual photon γ^* coupling to a given state are allowed to vary in the fit for various energy points, while the coupling constant parameters for the subsequent decay are taken as the common parameters for all energies. The conjugate modes share the same coupling constants. The masses, widths or Flatté parameters for the resonances of $f_0(500), f_0(980), f_2(1270), f_0(1370), \rho(1450)^\pm,$ and $\rho(1570)^\pm$ are fixed to the measured values from PDG [1], as given in Table 2. The mass and width of $b_1(1235)^\pm$ are floated due to large uncertainties. Then its nominal solution is fixed as the fitted result.

The significance of each intermediate state is estimated by the changes of $-2\ln\mathcal{L}$ and the number of degrees of freedom (NDF) after removing it from the simultaneous fit. We take the intermediate states with statistical significances greater than 5σ in two groups as the nominal solution, including $f_0(500), f_0(980), f_2(1270), f_0(1370), b_1(1235)^\pm,$ and $\rho(1450)^\pm,$ as shown in Fig. 5. It is found that the contributions from $f_0(500)$ and $b_1(1235)^\pm$ are the most significant, as shown in the $M_{\pi^+\pi^-}$ and $M_{\omega\pi^\pm}$ spectra, respectively. The statistical significances for various intermediate resonances are shown in Table 2.

Table 2. Masses, widths and statistical significances for various intermediate resonances in $e^+e^- \rightarrow \pi^+\pi^-\omega$.

Resonance	Mass (MeV/ c^2)	Width (MeV)	Group A	Group B
$f_0(500)$	507 (400~550)	475 (400~700)	27.8σ	22.8σ
$f_0(980)$	990 ± 20	—	10.9σ	6.4σ
$f_0(1370)$	1350 ± 150	200 ± 50	6.2σ	3.4σ
$f_2(1270)$	1275.5 ± 0.8	186.7 ± 2.2	9.3σ	5.4σ
$b_1(1235)^\pm$	1179.0 ± 9.0	255.8 ± 16.4	31.8σ	25.7σ
$\rho(1450)^\pm$	1465.0 ± 25	400 ± 60	4.7σ	6.9σ
$\rho(1570)^\pm$	1570 ± 70	144 ± 90	4.3σ	2.4σ
$\pi^+\pi^-\omega$	—	—	6.5σ	3.0σ

4.5 Fit results

For the simultaneous fit, the ratios and the signal yields of various intermediate states are obtained according to Eq. (4.13), as shown in Tables 4 and 5. And their statistical uncertainties are determined based on Eq. (4.14), in which the correlation among parameters is included. With the intermediate states in the nominal solution, we perform the simultaneous fit to the data samples for groups A and B. Taking the two data samples from $\sqrt{s} = 4.1780$ and 4.2263 GeV with large integrated luminosity as examples, Figs. 5 and 6 show the fit results for groups A and B, respectively.

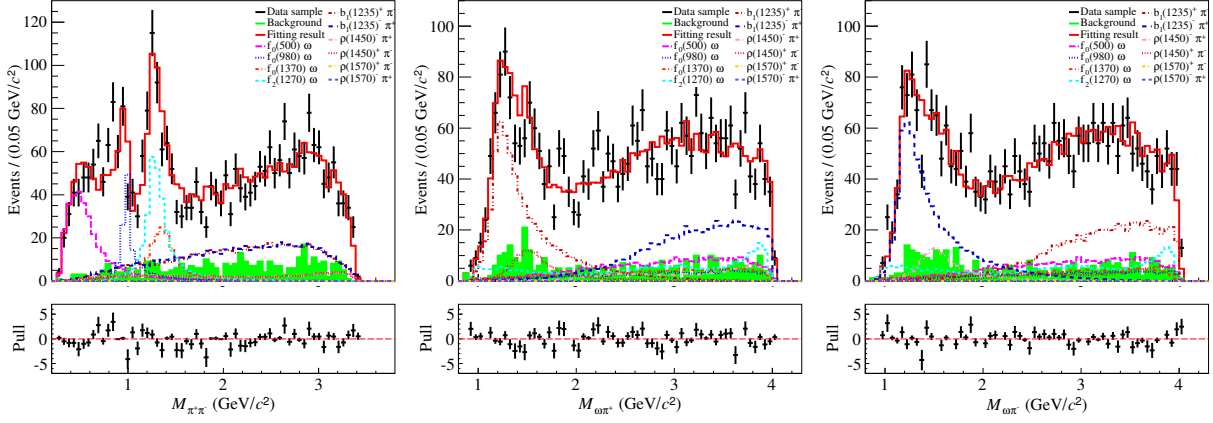


Figure 5. Projections of the PWA solution on the mass spectra $M_{\pi\pi}$, $M_{\omega\pi^+}$ and $M_{\omega\pi^-}$ for the data sample collected at $\sqrt{s} = 4.1780$ GeV. Points with error bars are data, the red histogram shows the final PWA fit results, and shaded histograms are the background estimated from the ω mass sideband regions. Other line shapes marked with different colors represent the fitted line shapes of different intermediate resonance states. The pull distribution of the fit result is shown at the bottom of each plot.

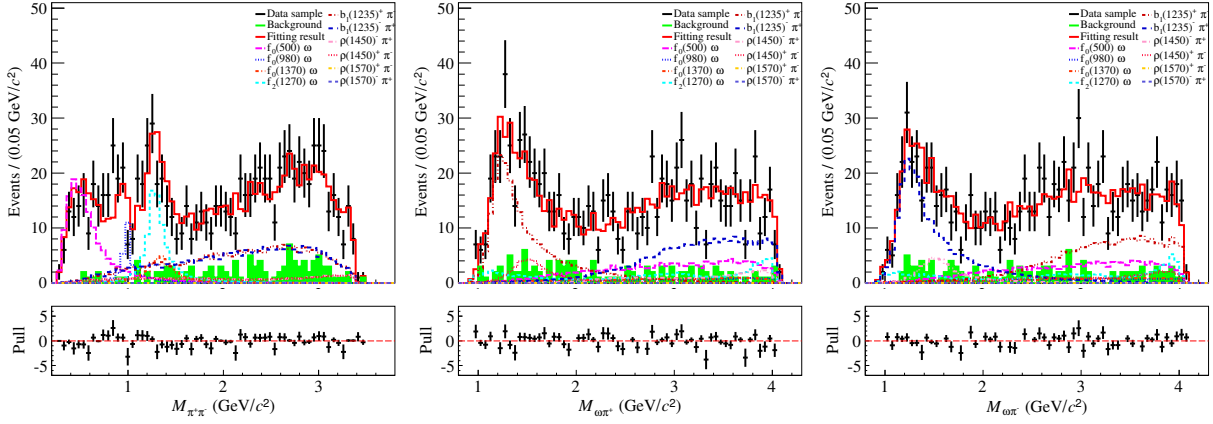


Figure 6. Projections of the PWA solution on the mass spectra $M_{\pi\pi}$, $M_{\omega\pi^+}$ and $M_{\omega\pi^-}$ for the data sample collected at $\sqrt{s} = 4.2263$ GeV. Points with error bars are data, the red histogram shows the final PWA fit results, and shaded histograms are the background estimated from the ω mass sideband regions. Other line shapes marked with different colors represent the fitted line shapes of different intermediate resonance states. The pull distribution of the fit result is shown at the bottom of each plot.

5 BORN CROSS SECTION

5.1 ISR correction factor

In e^+e^- collision experiments, the observed cross section, $\sigma_{\text{obs}}(s)$, at a c.m. energy point \sqrt{s} , is related to the corresponding Born cross section, $\sigma_0(s)$, by the ISR factor

$$1 + \delta = \frac{\sigma_{\text{obs}}(s)}{\sigma_0(s)}, \quad (5.1)$$

with

$$\sigma_{\text{obs}}(s) = \int_{M_{\text{th}}}^{\sqrt{s}} W(s, x) \frac{\sigma_0[s(1-x)]}{|1 - \Pi(\sqrt{s})|^2} dx, \quad (5.2)$$

where $\Pi(\sqrt{s})$ is the vacuum polarization (VP) function. The M_{th} corresponds to the $\pi^+\pi^-\omega$ mass threshold, and x is the effective fraction of the beam energy carried by photons emitted from the initial state, $x = \frac{2E_\gamma}{\sqrt{s}}$, and E_γ is the energy of the ISR photons. The initial state radiative function, $W(s, x)$, which uses the QED calculation up to next to leading order in Ref [70–72],

$$W(s, x) = \Delta \beta x^{\beta-1} - \frac{\beta}{2}(2-x) + \frac{\beta^2}{8} \left\{ (2-x)[3 \ln(1-x) - 4 \ln x] - 4 \frac{\ln(1-x)}{x} - 6 + x \right\}, \quad (5.3)$$

where

$$\begin{aligned} L &= 2 \ln \frac{\sqrt{s}}{m_e}, \\ \Delta &= 1 + \frac{\alpha}{\pi} \left(\frac{3}{2}L + \frac{1}{3}\pi^2 - 2 \right) + \left(\frac{\alpha}{\pi} \right)^2 \delta_2, \\ \delta_2 &= \left(\frac{9}{8} - 2\xi_2 \right) L^2 - \left(\frac{45}{16} - \frac{11}{2}\xi_2 - 3\xi_3 \right) L - \frac{6}{5}\xi_2^2 - \frac{9}{2}\xi_3 - 6\xi_2 \ln 2 + \frac{3}{8}\xi_2 + \frac{57}{12}, \\ \beta &= \frac{2\alpha}{\pi}(L-1), \quad \xi_2 = 1.64493407, \quad \xi_3 = 1.2020569, \end{aligned} \quad (5.4)$$

and we use the calculated results including the leptonic and hadronic parts both in the space-like and time-like region [73–77].

We use the generator model ConExc [61] to produce signal MC events and then iterate the Born cross-section measurement, in which the radiative function takes the result of high-order QED calculation up to the α^2 accuracy [71]. The Born cross sections from the $\pi^+\pi^-\omega$ mass threshold to 4.6 GeV are used to calculate the ISR factor. The Born cross sections $\sigma_0(s)$ in the c.m. energy ranges of below 3.0 GeV and (4.0, 4.6) GeV are taken from the measurements in Ref. [78] and this work, respectively. In the c.m. energy interval of (3.0, 4.0) GeV, however, the Born cross section of $e^+e^- \rightarrow$ continuum light hadrons is described by a polynomial, and the Born cross sections for J/ψ and $\psi(3686)$ are described by the function

$$\sigma(\sqrt{s}) = \frac{2J+1}{(2S_1+1)(2S_2+1)} \frac{4\pi}{k^2} \left[\frac{\Gamma^2/4}{(\sqrt{s} - \sqrt{s_0})^2 + \Gamma^2/4} \right] B_{\text{in}} B_{\text{out}}, \quad (5.5)$$

where \sqrt{s} is the c.m. energy, $J = 1$ is the spin of the resonance, and the numbers of polarization states of the two incident particles are $2S_1 + 1 = 2$ and $2S_2 + 1 = 2$, respectively. The maximum momentum of the final-state channel is denoted as k , $\sqrt{s_0}$ is the c.m. energy at the resonance, and Γ is the width of the resonance. The branching fractions of the resonance decays into the initial-state and final-state channels are denoted as B_{in} and B_{out} , respectively. The cross sections are smoothed by a fit to seven Gaussian functions in various energy intervals. Since the detection efficiency is affected by the radiative correction, an iteration over the cross section is done until the latest two results become stable; specifically, when the updated Born cross sections change by less than the statistical uncertainty. The ISR correction factor for each c.m. energy point is given in Table 3.

5.2 Born cross section of $e^+e^- \rightarrow \pi^+\pi^-\omega$

The Born cross section at each c.m. energy is calculated by

$$\sigma^{\text{Born}} = \frac{N^{\text{sig}}}{\mathcal{L}_{\text{int}} \cdot \epsilon \cdot (1 + \delta\gamma) \cdot \frac{1}{|1 - \Pi|^2} \cdot Br(\omega \rightarrow \pi^+\pi^-\pi^0) \cdot Br(\pi^0 \rightarrow \gamma\gamma)}, \quad (5.6)$$

where N^{sig} is the number of observed signal events, $(1 + \delta\gamma)$ and $\frac{1}{|1 - \Pi|^2}$ are the ISR correction and VP corrections, respectively. The factors $Br(\omega \rightarrow \pi^+\pi^-\pi^0)$ and $Br(\pi^0 \rightarrow \gamma\gamma)$ are the branching fractions of $\omega \rightarrow \pi^+\pi^-\pi^0$ and $\pi^0 \rightarrow \gamma\gamma$ from the PDG [1]. We use ϵ to denote the detection efficiency determined by the TOY MC sample with detector simulation of helicity amplitude model. The numerical results of Born cross sections are listed in Table 3.

5.3 Born cross section for intermediate states

The Born cross section for each intermediate state is calculated by

$$\sigma_i^{\text{Born}} = R_i \sigma^{\text{Born}}, \quad (5.7)$$

where σ^{Born} is the total Born cross section of $e^+e^- \rightarrow \pi^+\pi^-\omega$, including the interference contributions among all intermediate states. The cross-section ratio, R_i , is calculated according to Eq. (4.13) and given in Table 4, and the Born cross section of each intermediate state is shown in Fig. 7.

6 SYSTEMATIC UNCERTAINTY

6.1 Uncertainty of the Born cross section

The uncertainties in the Born cross section measurements arise from the luminosity measurement, tracking and PID efficiency, photon detection efficiency, branching fraction, K_S^0 veto, ISR correction, fit procedure, PWA, and insignificant resonances. However, the effects of the E_{EMC}/p requirement and χ_{c0} veto on efficiency are negligible.

- *Luminosity.* The integrated luminosity is measured by the Bhabha scattering process, and the uncertainty is 1.0% [55].

Table 3. Integrated luminosities (\mathcal{L}_{int}), detection efficiencies (ϵ), signal yields (N^{sig}), ISR factors ($1 + \delta^\gamma$), VP factors ($\frac{1}{|1 - \Pi|^2}$), and the obtained Born cross sections (σ^{Born}) at different c.m. energies (\sqrt{s}). The first uncertainties for Born cross sections are statistical and the second are systematic.

\sqrt{s} (GeV)	\mathcal{L}_{int} (pb $^{-1}$)	ϵ (%)	N^{sig}	$(1 + \delta^\gamma)$	$\frac{1}{ 1 - \Pi ^2}$	σ^{Born} (pb)
4.0076	482.0	3.9	634 \pm 28	4.5	1.0435	8.1 \pm 0.4 \pm 0.6
4.1285	393.4	4.4	408 \pm 23	4.6	1.0526	5.5 \pm 0.3 \pm 0.5
4.1574	406.9	4.2	398 \pm 22	4.8	1.0535	5.1 \pm 0.3 \pm 0.5
4.1780	3194.5	4.1	2888 \pm 60	4.8	1.0548	4.9 \pm 0.1 \pm 0.5
4.1890	523.9	4.2	452 \pm 24	4.8	1.0560	4.6 \pm 0.2 \pm 0.4
4.1990	525.2	4.2	462 \pm 26	4.9	1.0568	4.6 \pm 0.3 \pm 0.5
4.2093	517.2	4.1	467 \pm 24	4.8	1.0565	4.9 \pm 0.3 \pm 0.5
4.2188	513.4	4.3	444 \pm 24	4.9	1.0565	4.5 \pm 0.2 \pm 0.4
4.2263	1056.4	3.9	909 \pm 34	4.9	1.0548	4.8 \pm 0.2 \pm 0.4
4.2358	529.1	4.0	427 \pm 23	5.0	1.0554	4.3 \pm 0.2 \pm 0.4
4.2439	536.3	4.3	459 \pm 24	5.0	1.0552	4.4 \pm 0.2 \pm 0.4
4.2580	828.4	3.9	670 \pm 30	5.0	1.0533	4.5 \pm 0.2 \pm 0.4
4.2668	529.7	3.8	430 \pm 13	5.0	1.0531	4.5 \pm 0.1 \pm 0.4
4.2777	175.2	3.7	131 \pm 14	5.1	1.0529	4.3 \pm 0.5 \pm 0.5
4.2879	491.5	3.9	421 \pm 23	5.1	1.0525	4.6 \pm 0.3 \pm 0.4
4.3121	492.1	3.7	366 \pm 22	5.2	1.0519	4.2 \pm 0.3 \pm 0.5
4.3374	501.1	3.7	390 \pm 22	5.2	1.0508	4.3 \pm 0.2 \pm 0.5
4.3583	543.9	3.7	377 \pm 22	5.3	1.0511	3.8 \pm 0.2 \pm 0.3
4.3774	522.8	3.8	406 \pm 22	5.4	1.0514	4.1 \pm 0.2 \pm 0.3
4.3965	505.0	3.4	255 \pm 18	5.4	1.0517	2.9 \pm 0.2 \pm 0.3
4.4156	1043.9	3.7	716 \pm 30	5.4	1.0524	3.7 \pm 0.2 \pm 0.3
4.4362	568.1	3.7	365 \pm 21	5.5	1.0543	3.4 \pm 0.2 \pm 0.4
4.4671	111.1	3.6	80 \pm 10	5.6	1.0548	3.8 \pm 0.5 \pm 0.4
4.5995	586.9	3.1	259 \pm 18	6.1	1.0547	2.5 \pm 0.2 \pm 0.2

- *Tracking and PID efficiencies.* The uncertainty of the tracking efficiency has been studied with a high purity control sample of $e^+e^- \rightarrow \pi^+\pi^-K^+K^-$ [79]. The differences of the tracking and PID efficiencies between data and MC simulation in different transverse momentum and momentum ranges are taken as the systematic uncertainties of tracking and PID efficiencies, both 1.0% per charged pion.
- *Photon detection efficiency.* The uncertainty from the photon detection has been studied with the control samples of $\psi(3686) \rightarrow \pi^0\pi^0J/\psi$ and $e^+e^- \rightarrow \omega\pi^0 \rightarrow \pi^+\pi^-\pi^0\pi^0$ [79], which is 1.0% per photon.
- *Branching fraction.* The branching fractions $Br(\omega \rightarrow \pi^+\pi^-\pi^0)$ and $Br(\pi^0 \rightarrow \gamma\gamma)$ are quoted from the PDG [1], which are (89.2 \pm 0.7)% and (98.823 \pm 0.034)%, respectively. The relevant systematic uncertainty is 0.75% in total.
- *K_S^0 veto.* The uncertainty of K_S^0 veto is taken as the difference of efficiencies with and without K_S^0 veto between data and MC simulation, which is 0.8%.

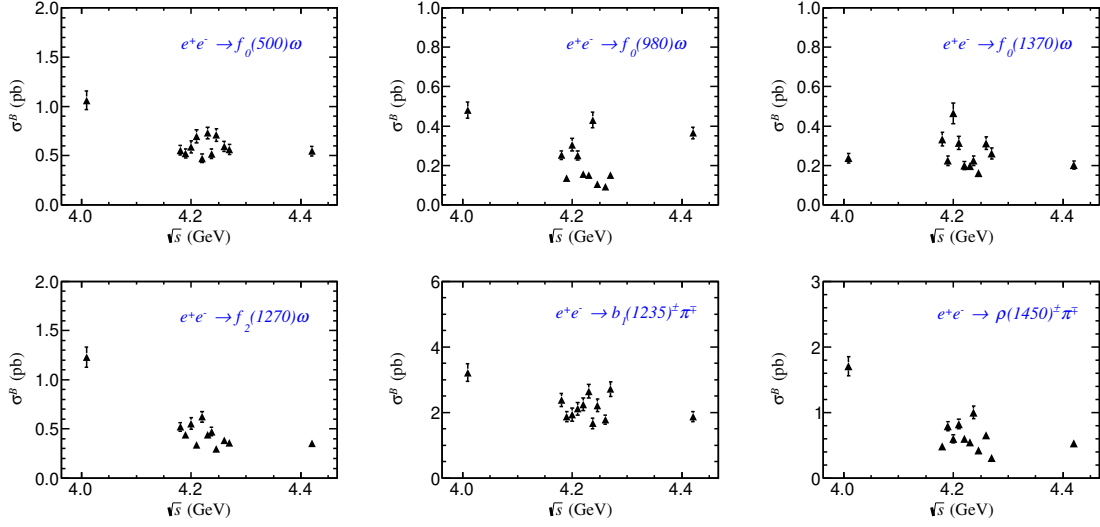


Figure 7. The Born cross sections of the processes containing $f_0(500)$, $f_0(980)$, $f_2(1270)$, $f_0(1370)$, $b_1(1235)^\pm$, and $\rho(1450)^\pm$. Uncertainties combine both statistical and systematic uncertainties.

Table 4. The ratios of signal yields for intermediate states ($f_0(500)$, $f_0(980)$, $f_2(1270)$, $f_0(1370)$, $b_1(1235)^\pm$, $\rho(1450)^\pm$), and non-resonant $\pi^+\pi^-\omega$ at different c.m. energy points, which are divided into groups A and B for higher statistics.

Group	\sqrt{s} (GeV)	$f_0(500)$	$f_0(980)$	$f_0(1370)$	$f_2(1270)$	$b_1(1235)^\pm$	$\rho(1450)^\pm$	$\pi^+\pi^-\omega$
A	4.0076	0.13 ± 0.02	0.06 ± 0.02	0.03 ± 0.02	0.15 ± 0.03	0.40 ± 0.05	0.21 ± 0.04	0.00 ± 0.01
	4.1780	0.11 ± 0.01	0.05 ± 0.01	0.07 ± 0.01	0.11 ± 0.01	0.48 ± 0.02	0.10 ± 0.02	0.09 ± 0.02
	4.1890	0.11 ± 0.02	0.03 ± 0.02	0.05 ± 0.03	0.09 ± 0.03	0.40 ± 0.05	0.17 ± 0.04	0.12 ± 0.04
	4.1990	0.13 ± 0.02	0.07 ± 0.03	0.10 ± 0.04	0.12 ± 0.04	0.42 ± 0.05	0.13 ± 0.04	0.09 ± 0.03
	4.2093	0.14 ± 0.03	0.05 ± 0.03	0.06 ± 0.04	0.07 ± 0.03	0.43 ± 0.05	0.17 ± 0.05	0.06 ± 0.03
	4.2188	0.11 ± 0.02	0.03 ± 0.02	0.04 ± 0.03	0.14 ± 0.03	0.51 ± 0.06	0.13 ± 0.05	0.06 ± 0.03
B	4.2263	0.15 ± 0.02	0.03 ± 0.01	0.04 ± 0.02	0.09 ± 0.02	0.56 ± 0.04	0.11 ± 0.03	0.03 ± 0.03
	4.2358	0.12 ± 0.03	0.10 ± 0.03	0.05 ± 0.04	0.11 ± 0.02	0.39 ± 0.05	0.24 ± 0.03	0.05 ± 0.03
	4.2439	0.16 ± 0.03	0.02 ± 0.02	0.04 ± 0.02	0.07 ± 0.02	0.51 ± 0.05	0.10 ± 0.04	0.10 ± 0.04
	4.2580	0.13 ± 0.02	0.02 ± 0.01	0.07 ± 0.03	0.09 ± 0.02	0.40 ± 0.04	0.15 ± 0.03	0.11 ± 0.03
	4.2668	0.12 ± 0.02	0.03 ± 0.02	0.06 ± 0.04	0.08 ± 0.03	0.60 ± 0.07	0.07 ± 0.04	0.03 ± 0.03
	4.4156	0.15 ± 0.02	0.10 ± 0.03	0.05 ± 0.03	0.10 ± 0.02	0.51 ± 0.05	0.14 ± 0.04	0.01 ± 0.01

- *ISR correction.* To obtain reliable detection efficiencies, the Born cross sections input in the generator have been iterated until the $(1+\delta^r)\cdot\epsilon$ values converge. The differences of $(1+\delta^r)\cdot\epsilon$ between the last two iterations are taken as the corresponding systematic uncertainties.
- *Fit procedure.* The systematic uncertainty in the fit of $M_{\pi^+\pi^-\pi^0}$ mainly comes from the fit range, signal shape and background shape. The fit range is changed from $[0.68, 0.91]$ GeV/ c^2 to $[0.67, 0.92]$ GeV/ c^2 . The signal shape is changed to the *BW* function

Table 5. The signal yields for intermediate states ($f_0(500)$, $f_0(980)$, $f_2(1270)$, $f_0(1370)$, $b_1(1235)^\pm$, and $\rho(1450)^\pm$) at different c.m. energy points, which are divided into groups A and B for higher statistics. The errors are statistical only.

Group	\sqrt{s} (GeV)	$f_0(500)$	$f_0(980)$	$f_0(1370)$	$f_2(1270)$	$b_1(1235)^\pm$	$\rho(1450)^\pm$
A	4.0076	77.40 ± 13.51	34.88 ± 12.36	17.21 ± 12.15	89.32 ± 15.50	233.49 ± 26.19	123.89 ± 23.47
	4.1780	298.92 ± 28.95	136.22 ± 29.90	179.80 ± 40.13	281.23 ± 37.93	1284.20 ± 63.06	260.12 ± 42.96
	4.1890	47.14 ± 10.67	12.28 ± 11.92	20.31 ± 13.80	39.90 ± 13.47	170.09 ± 19.53	71.91 ± 17.73
	4.1990	53.41 ± 11.19	27.73 ± 14.27	42.27 ± 16.92	50.58 ± 15.52	176.50 ± 19.13	54.62 ± 16.57
	4.2093	59.40 ± 12.32	21.34 ± 11.31	26.77 ± 17.14	28.84 ± 13.23	180.88 ± 19.48	70.47 ± 19.60
	4.2188	42.73 ± 10.00	13.99 ± 9.97	17.97 ± 13.92	56.45 ± 13.82	203.56 ± 22.39	54.25 ± 19.80
B	4.2263	128.26 ± 17.67	26.69 ± 12.74	34.71 ± 18.75	77.60 ± 17.80	466.33 ± 33.06	95.40 ± 24.50
	4.2358	47.61 ± 12.54	39.58 ± 13.21	20.56 ± 15.28	43.47 ± 10.32	153.61 ± 20.45	92.14 ± 19.50
	4.2439	68.69 ± 11.56	9.99 ± 7.78	15.42 ± 11.29	28.71 ± 11.16	214.59 ± 20.95	41.08 ± 18.88
	4.2580	81.67 ± 15.42	12.52 ± 8.91	43.09 ± 16.44	53.24 ± 14.53	246.22 ± 24.71	89.86 ± 21.01
	4.2668	49.34 ± 11.15	13.15 ± 8.74	22.76 ± 16.21	31.61 ± 13.65	237.85 ± 26.53	27.10 ± 18.16
	4.4156	96.94 ± 16.25	64.90 ± 20.71	35.83 ± 26.22	62.95 ± 17.77	334.32 ± 28.10	94.23 ± 24.30

convolved with a Gaussian resolution function. The background shape is changed from the second-order Chebyshev polynomial to the third-order, and the parameter of the background function is fixed to that derived from the fit to the largest data sample taken at $\sqrt{s} = 4.178$ GeV. The quadrature sum of the changes in the fitted signal yield is taken as the uncertainty.

- *PWA.* The uncertainties due to the mass and width of the intermediate resonance state, the background level, and the kinematic fit are considered in the systematic uncertainty of PWA. The main contribution comes from $f_0(500)$, $f_0(980)$, $f_2(1270)$, $b_1(1235)^\pm$, and $\rho(1450)^\pm$. The total uncertainty is the sum of the following three detailed sources.
- *Mass and width.* The masses and widths of the intermediate resonance states in this analysis are fixed on the PDG values [1]. To estimate their systematic uncertainties, we shift the mass and width of each intermediate resonance within one standard deviation.
- *Background level.* The background level is determined by the ω sideband events of the data sample. It is the same size as the number of events obtained in the ω signal region after the integration of the background function. To estimate the systematic uncertainty of the background level, we determine the deviation of the background level according to $\Delta n = \sqrt{N}$, where N is the estimated number of the background events in the ω signal region, and change the background yield by $(N + \Delta n)$.
- *Kinematic fit.* The uncertainty of the kinematic fit is estimated by correcting the helix parameters of the charged tracks to improve the consistency between TOY data and MC simulation [80]. The difference in the detection efficiencies of the TOY MC samples is regarded as the systematic uncertainty in PWA.

- *Insignificant resonance.* An intermediate state with significance less than 5σ , $\rho(1570)^\pm$, is removed in the normal solution. The uncertainty is defined as the difference between the detection efficiencies of the normal solution with and without the $\rho(1570)^\pm$ contribution.

The numerical values of these systematic uncertainties are summarized in Table 6. For the total uncertainty these contributions are added in quadrature.

6.2 Uncertainty of the Born cross section for intermediate process

The systematic uncertainty in the measurements of the Born cross sections for the intermediate processes is the same as that of $e^+e^- \rightarrow \pi^+\pi^-\omega$. Whereas, for the Born cross section measurement of intermediate state, the uncertainty in PWA depends on the ratio of each intermediate state, R_i . We mainly estimate the systematic uncertainty of the Born cross section of different intermediate processes for the twelve c.m. energy points with higher statistics. Their uncertainties are obtained by adding the individual contributions in quadrature and summarized in Table 7.

- *Mass and width.* For the uncertainties of the mass and width of any of the intermediate resonance states, we change its mass and width according to the PDG values within $\pm 1\sigma$.
- *Background level.* We determine the deviation of the background level according to n_i , and change the background yield to obtain the uncertainty of the background level.
- *Kinematic fit.* We use the PHSP signal MC sample corrected by the helix parameters to re-perform PWA to estimate the uncertainty of the kinematic fit.
- *Insignificant resonance.* The uncertainty due to one insignificant resonance was defined as the difference between the ratio of the normal solution with and without the $\rho(1570)^\pm$ contribution.

For each source, the deviation from the nominal result is taken as the corresponding systematic uncertainty.

7 FIT TO THE LINE SHAPE

The line shape for total Born cross section of $e^+e^- \rightarrow \pi^+\pi^-\omega$ is fitted with the least square method [81]. First, the energy-dependent Born cross section is parameterized by a non-resonant function $f(\sqrt{s}) = a/s^n$, where a and n are free parameters. The correlations among different c.m. energy points are considered in the fit with the χ^2 defined as below (and minimized by MINUIT [67]),

$$\chi^2 = \sum_i \frac{(\sigma_{B_i} - \sigma_{B_i}^{\text{fit}})^2}{\delta_i^2}, \quad (7.1)$$

Table 6. Relative systematic uncertainties (in %) in the cross section measurements include the luminosity(Lum), the tracking efficiency (Trk), the PID, the photon detection (PD), the branching fraction (BF), the veto of K_S^0 (K_S^V), the ISR correction (ISR), the signal shape (SS), the background shape (BS), the fit range (FR), PWA, and insignificant resonance (IR). The sources with a superscript * are the common systematic uncertainties for different c.m. energies.

\sqrt{s} (GeV)	Lum*	Trk*	PID*	PD*	BF*	K_S^V *	ISR	SS	BS	FR	PWA	IR	Total
4.0076	1.0	4.0	4.0	2.0	0.75	0.8	1.1	0.8	1.1	0.6	0.3	3.1	7.2
4.1285	1.0	4.0	4.0	2.0	0.75	0.8	2.8	0.7	0.7	1.0	0.2	4.1	8.1
4.1574	1.0	4.0	4.0	2.0	0.75	0.8	1.5	1.0	1.5	0.0	4.8	0.4	8.2
4.1780	1.0	4.0	4.0	2.0	0.75	0.8	5.2	0.6	1.1	0.7	0.0	1.7	8.4
4.1890	1.0	4.0	4.0	2.0	0.75	0.8	0.7	0.9	0.7	0.0	3.5	3.0	7.8
4.1990	1.0	4.0	4.0	2.0	0.75	0.8	5.5	0.0	1.5	0.7	2.6	4.6	10.0
4.2093	1.0	4.0	4.0	2.0	0.75	0.8	3.9	0.6	0.9	1.2	2.7	2.6	8.3
4.2188	1.0	4.0	4.0	2.0	0.75	0.8	1.0	0.7	0.9	1.1	1.7	5.8	8.9
4.2263	1.0	4.0	4.0	2.0	0.75	0.8	0.6	0.3	1.3	0.4	1.3	3.9	7.6
4.2358	1.0	4.0	4.0	2.0	0.75	0.8	3.6	0.2	0.9	1.9	2.1	2.9	8.3
4.2439	1.0	4.0	4.0	2.0	0.75	0.8	1.5	0.7	1.1	0.7	0.8	3.1	7.3
4.2580	1.0	4.0	4.0	2.0	0.75	0.8	0.8	1.4	1.5	1.1	2.7	1.4	7.3
4.2668	1.0	4.0	4.0	2.0	0.75	0.8	1.1	0.2	1.2	0.0	1.5	4.0	7.7
4.2777	1.0	4.0	4.0	2.0	0.75	0.8	4.7	0.0	1.5	0.0	1.5	4.6	9.3
4.2879	1.0	4.0	4.0	2.0	0.75	0.8	2.7	0.5	1.0	0.5	0.2	1.0	6.9
4.3121	1.0	4.0	4.0	2.0	0.75	0.8	5.9	0.6	1.6	1.1	0.9	5.0	10.1
4.3374	1.0	4.0	4.0	2.0	0.75	0.8	6.8	1.0	0.5	0.5	3.0	1.1	9.8
4.3583	1.0	4.0	4.0	2.0	0.75	0.8	3.2	1.1	1.3	1.6	1.1	2.5	7.8
4.3774	1.0	4.0	4.0	2.0	0.75	0.8	0.0	0.5	1.0	1.5	0.2	0.5	6.5
4.3965	1.0	4.0	4.0	2.0	0.75	0.8	2.9	0.4	0.8	0.0	2.0	1.2	7.3
4.4156	1.0	4.0	4.0	2.0	0.75	0.8	1.4	0.3	0.8	0.9	1.7	3.2	7.4
4.4362	1.0	4.0	4.0	2.0	0.75	0.8	5.5	0.8	1.1	0.8	3.3	0.1	9.0
4.4671	1.0	4.0	4.0	2.0	0.75	0.8	3.8	0.0	1.3	1.3	2.8	5.6	9.7
4.5995	1.0	4.0	4.0	2.0	0.75	0.8	1.6	0.8	1.1	1.6	3.0	2.4	7.7

where σ_{B_i} and $\sigma_{B_i}^{\text{fit}}$ are the measured and fitted values for Born cross section at the i -th c.m. energy point, respectively. here, δ_i is the uncertainty for the i -th c.m. energy point, which includes the statistical uncertainty and the uncorrelated part of the systematic uncertainty. Figure 8 shows the fit result with $\chi^2/\text{NDF} = 27.75/(24 - 2 - 1) \approx 1.32$.

Secondly, the Born cross section is parameterized as the coherent sum of the energy-dependent non-resonant function and one charmonium or charmonium-like state amplitude,

$$\sigma^{\text{Born}}(\sqrt{s}) = |BW(\sqrt{s})e^{i\phi} + \sqrt{f(\sqrt{s})}|^2, \quad (7.2)$$

where $f(\sqrt{s})$ denotes the non-resonant amplitude, ϕ is the relative phase between the continuum and resonant amplitudes, and $BW(\sqrt{s})$ is a relativistic BW function which is used to describe the charmonium states, $BW(\sqrt{s}) = \frac{\sqrt{12}\pi\Gamma_{ee}Br\Gamma_{\text{tot}}}{s-M^2+iM\Gamma_{\text{tot}}}$. And since these energies are far from the threshold of the $e^+e^- \rightarrow \pi^+\pi^-\omega$ process, the effect of the three-

Table 7. The systematic uncertainties (in %) in the cross section measurements of the intermediate processes containing $f_0(500)$, $f_0(980)$, $f_2(1270)$, $f_0(1370)$, $b_1(1235)^\pm$, and $\rho(1450)^\pm$. The results of simultaneous to groups A and B, which are combined from twelve c.m. energy points for higher statistics.

Group	\sqrt{s} (GeV)	$f_0(500)$	$f_0(980)$	$f_0(1370)$	$f_2(1270)$	$b_1(1235)^\pm$	$\rho(1450)^\pm$
A	4.0076	7.9	7.1	9.1	7.2	7.2	7.1
	4.1780	8.5	8.3	10.3	8.3	8.3	8.2
	4.1890	7.0	6.5	9.4	6.5	6.5	6.4
	4.1990	8.7	8.7	10.1	8.7	8.7	8.6
	4.2093	7.7	7.5	9.3	7.5	7.6	7.5
	4.2188	7.2	6.9	9.0	6.9	6.9	6.8
B	4.2263	6.9	6.6	8.4	6.6	6.6	6.5
	4.2358	7.9	7.7	9.6	7.7	7.7	7.6
	4.2439	7.3	6.6	8.9	6.6	6.7	6.6
	4.2580	7.3	6.7	9.3	6.6	6.7	6.8
	4.2668	8.5	7.5	10.2	7.5	7.6	7.9
	4.4156	7.6	6.9	9.2	6.8	6.9	7.1

body phase space factor is very small and therefore this $BW(\sqrt{s})$ function omits it. The symbols M , Br , Γ_{ee} , and Γ_{tot} denote the mass, the branching fraction of $Y \rightarrow \pi^+\pi^-\omega$, the partial width to e^+e^- , and the total width, respectively. The considered charmonium and charmonium-like states include $\psi(4160)$, $Y(4220)$, $Y(4360)$, and $\psi(4415)$. In the fit, these resonance states are individually fitted with fixed mass and width from the PDG. The fit results are shown in Fig. 8. The goodness-of-fit tests for $\psi(4160)$, $Y(4220)$, $Y(4360)$, and $\psi(4415)$ yield $\chi^2/\text{NDF} = 19.8/19$, $21.4/19$, $26.4/19$, and $26.6/19$, respectively. The fit has two solutions with equal fit quality. The fitted parameters of various resonance states are shown in Table 8. The statistical significances of $\psi(4160)$ and $Y(4220)$ are 3.6σ and 3.1σ , while those of $Y(4360)$ and $\psi(4415)$ are 1.1σ and 1.0σ , respectively.

Table 8. Fitted parameters and statistical significances for various charmonium states decaying into $\pi^+\pi^-\omega$. The uncertainties are statistical only.

Parameter	$\psi(4160)$		$Y(4220)$	
	Solution I	Solution II	Solution I	Solution II
$12\pi\Gamma_{ee}Br$ (eV)	0.03 ± 0.02	24.57 ± 0.47	18.29 ± 0.32	0.02 ± 0.02
Γ_{tot} (GeV)	0.070		0.055	
M (GeV/ c^2)	4.191		4.23	
ϕ (rad)	4.61 ± 0.34	4.68 ± 0.01	4.70 ± 0.01	5.38 ± 0.31
Significance (σ)	3.6		3.1	

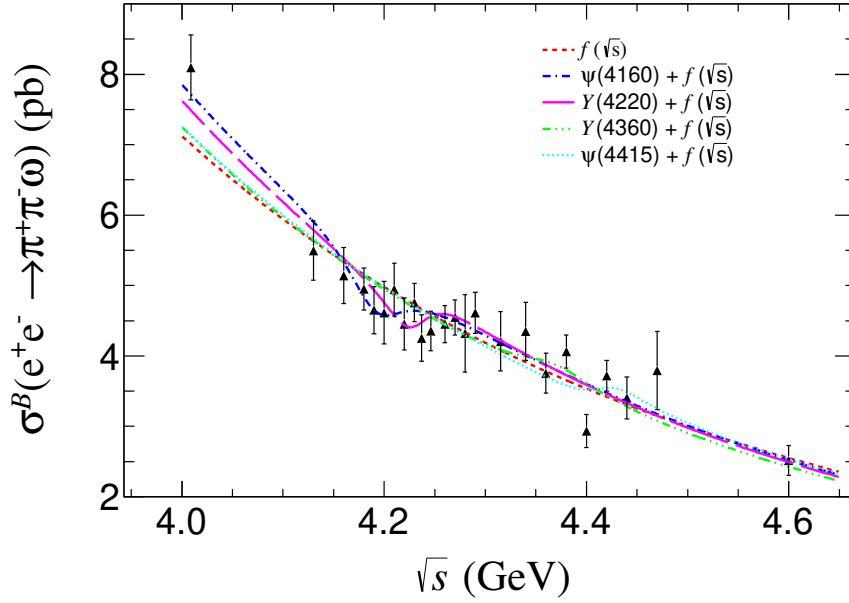


Figure 8. Fitted results of the measured Born cross sections at c.m. energies between 4.0 and 4.6 GeV. The data are presented as filled triangles with error bars combining statistical and uncorrelated systematic uncertainties. The curves are the fit results to various amplitudes as described in the text.

8 SUMMARY

In conclusion, the process of $e^+e^- \rightarrow \pi^+\pi^-\omega$ is studied at twenty-four c.m. energies in the region from 4.0 to 4.6 GeV. The Born cross sections of $e^+e^- \rightarrow \pi^+\pi^-\omega$ and the intermediate state production at twelve c.m. energy points are measured with helicity amplitude analysis method. The results indicate that the dominant contributions are from $e^+e^- \rightarrow f_0(500)\omega$, $f_0(980)\omega$, $f_2(1270)\omega$, $f_0(1370)\omega$, $b_1(1235)^\pm\pi^\mp$, $\rho(1450)^\pm\pi^\mp$ with statistical significances greater than 5σ . By analyzing the line shape of the Born cross section of the $e^+e^- \rightarrow \pi^+\pi^-\omega$ process, greater than 3σ evidence for a state with mass about 4.2 GeV/ c^2 is found, which is consistent with the production of either $\psi(4160)$ or $Y(4220)$.

Acknowledgments

The BESIII collaboration thanks the staff of BEPCII and the IHEP computing center for their strong support. This work is supported in part by National Key R&D Program of China under Contracts Nos. 2020YFA0406300, 2020YFA0406400; National Natural Science Foundation of China (NSFC) under Contracts Nos. 11975118, 12175244, 11875262, 11635010, 11735014, 11835012, 11935015, 11935016, 11935018, 11961141012, 12022510, 12025502, 12035009, 12035013, 12192260, 12192261, 12192262, 12192263, 12192264, 12192265, 12061131003; the Science and Technology Innovation Program of Hunan Province under Contract No. 2020RC3054; the Chinese Academy of Sciences (CAS) Large-Scale Scientific

Facility Program; Joint Large-Scale Scientific Facility Funds of the NSFC and CAS under Contract No. U1832207; the CAS Center for Excellence in Particle Physics (CCEPP); 100 Talents Program of CAS; The Institute of Nuclear and Particle Physics (INPAC) and Shanghai Key Laboratory for Particle Physics and Cosmology; ERC under Contract No. 758462; European Union’s Horizon 2020 research and innovation programme under Marie Skłodowska-Curie grant agreement under Contract No. 894790; German Research Foundation DFG under Contracts Nos. 443159800, Collaborative Research Center CRC 1044, GRK 2149; Istituto Nazionale di Fisica Nucleare, Italy; Ministry of Development of Turkey under Contract No. DPT2006K-120470; National Science and Technology fund; National Science Research and Innovation Fund (NSRF) via the Program Management Unit for Human Resources & Institutional Development, Research and Innovation under Contract No. B16F640076; STFC (United Kingdom); Suranaree University of Technology (SUT), Thailand Science Research and Innovation (TSRI), and National Science Research and Innovation Fund (NSRF) under Contract No. 160355; The Royal Society, UK under Contracts Nos. DH140054, DH160214; The Swedish Research Council; U. S. Department of Energy under Contract No. DE-FG02-05ER41374

References

- [1] P.A. Zyla *et al.* [Particle Data Group], *Review of Particle Physics*, *Prog. Theor. Exp. Phys.* **2020** (2020) 083C01.
- [2] S.K. Choi *et al.* [Belle Collaboration], *Observation of a narrow charmonium-like state in exclusive $B^\pm \rightarrow K^\pm \pi^+ \pi^- J/\psi$ decays*, *Phys. Rev. Lett.* **91** (2003) 262001 [[arXiv:hep-ex/0309032](#)] [[INSPIRE](#)].
- [3] B. Aubert *et al.* [BaBar Collaboration], *Observation of a Broad Structure in the $\pi^+ \pi^- J/\psi$ Mass Spectrum around $4.26 \text{ GeV}/c^2$* , *Phys. Rev. Lett.* **95** (2005) 142001 [[arXiv:hep-ex/0506081](#)] [[INSPIRE](#)].
- [4] M. Ablikim *et al.* [BESIII Collaboration], *Observation of a Charged Charmoniumlike Structure in $e^+ e^- \rightarrow \pi^+ \pi^- J/\psi$ at $\sqrt{s}=4.26 \text{ GeV}$* , *Phys. Rev. Lett.* **110** (2013) 252001 [[arXiv:1303.5949](#)] [[INSPIRE](#)].
- [5] S.K. Choi *et al.* [Belle Collaboration], *Study of $e^+ e^- \rightarrow \pi^+ \pi^- J/\psi$ and Observation of a Charged Charmoniumlike State at Belle*, *Phys. Rev. Lett.* **110** (2013) 252002 [[arXiv:1304.0121](#)] [[INSPIRE](#)].
- [6] Q. He *et al.* [CLEO Collaboration], *Confirmation of the $Y(4260)$ resonance production in ISR*, *Phys. Rev. D* **74** (2006) 091104 [[arXiv:hep-ex/0611021](#)] [[INSPIRE](#)].
- [7] C. Z. Yuan *et al.* [Belle Collaboration], *Measurement of $e^+ e^- \rightarrow \pi^+ \pi^- J/\psi$ cross-section via initial state radiation at Belle*, *Phys. Rev. Lett.* **99** (2007) 182004 [[arXiv:0707.2541](#)] [[INSPIRE](#)].
- [8] M. Ablikim *et al.* [BESIII Collaboration], *Precise Measurement of the Cross Section at $e^+ e^- \rightarrow \pi^+ \pi^- J/\psi$ Center-of-Mass Energies from 3.77 to 4.60 GeV*, *Phys. Rev. Lett.* **118** (2017) 092001 [[arXiv:1611.01317](#)] [[INSPIRE](#)].
- [9] M. Ablikim *et al.* [BESIII Collaboration], *Study of $e^+ e^- \rightarrow \omega \chi_{cJ}$ at center-of-mass energies from 4.21 to 4.42 GeV*, *Phys. Rev. Lett.* **114** (2015) 092003 [[arXiv:1410.6538](#)] [[INSPIRE](#)].

- [10] M. Ablikim *et al.* [BESIII Collaboration], *Evidence of Two Resonant Structures in $e^+e^- \rightarrow \pi^+\pi^-h_c$* , *Phys. Rev. Lett.* **118** (2017) 092002 [arXiv:1610.07044] [INSPIRE].
- [11] M. Ablikim *et al.* [BESIII Collaboration], *Measurement of $e^+e^- \rightarrow \pi^+\pi^-\psi(3686)$ from 4.008 to 4.600 GeV and observation of a charged structure in the $\pi^\pm\psi(3686)$ mass spectrum*, *Phys. Rev. D* **96** (2017) 032004 [arXiv:1703.08787] [INSPIRE].
- [12] M. Ablikim *et al.* [BESIII Collaboration], *Evidence of a resonant structure in the $e^+e^- \rightarrow \pi^+D^0D^{*-}$ cross section between 4.05 and 4.60 GeV*, *Phys. Rev. Lett.* **122** (2019) 102002 [arXiv:1808.02847] [INSPIRE].
- [13] B. Aubert *et al.* [BaBar Collaboration], *Evidence of a broad structure at an invariant mass of 4.32 GeV/c² in the reaction $e^+e^- \rightarrow \pi^+\pi^-\psi_{2S}$ measured at BaBar*, *Phys. Rev. Lett.* **98** (2007) 212001 [arXiv:hep-ex/0610057] [INSPIRE].
- [14] S.K. Choi *et al.* [Belle Collaboration], *Observation of Two Resonant Structures in $e^+e^- \rightarrow \pi^+\pi^-\psi(2S)$ via Initial State Radiation at Belle*, *Phys. Rev. Lett.* **99** (2007) 142002 [arXiv:0707.3699] [INSPIRE].
- [15] H. X. Chen *et al.*, *The hidden-charm pentaquark and tetraquark states*, *Phys. Rept.* **639** (2016) 1 [arXiv:1601.02092] [INSPIRE].
- [16] Y. R. Liu *et al.*, *Pentaquark and Tetraquark states*, *Prog. Part. Nucl. Phys.* **107** (2019) 237 [arXiv:1903.11976] [INSPIRE].
- [17] L. Maiani *et al.*, *Four quark interpretation of $Y(4260)$* , *Phys. Rev. D* **72** (2005) 031502 [arXiv:hep-ph/0507062] [INSPIRE].
- [18] A. Ali *et al.*, *A new look at the Y tetraquarks and Ω_c baryons in the diquark model*, *Eur. Phys. J. C* **78** (2018) 29 [arXiv:1708.04650] [INSPIRE].
- [19] S.J. Brodsky *et al.*, *A New Picture for the Formation and Decay of the Exotic XYZ Mesons*, *Phys. Rev. Lett.* **113** (2014) 112001 [arXiv:1406.7281] [INSPIRE].
- [20] J.R. Zhang and M.Q. Huang, *The P-wave $[cs][\bar{c}\bar{s}]$ tetraquark state: $Y(4260)$ or $Y(4660)$?*, *Phys. Rev. D* **83** (2011) 036005 [arXiv:1011.2818] [INSPIRE].
- [21] J.R. Zhang and M.Q. Huang, *Could $Y_b(10890)$ be the P-wave $[bq][\bar{b}\bar{q}]$ tetraquark state?*, *JHEP* **11** (2010) 057 [arXiv:1011.2815] [INSPIRE].
- [22] Z.G. Wang, *Tetraquark state candidates: $Y(4260)$, $Y(4360)$, $Y(4660)$ and $Z_c(4020/4025)$* , *Eur. Phys. J. C* **76** (2016) 387 [arXiv:1601.05541] [INSPIRE].
- [23] N. Brambilla *et al.*, *Heavy quarkonium: progress, puzzles, and opportunities*, *Eur. Phys. J. C* **71** (2011) 1534 [arXiv:arXiv:1010.5827] [INSPIRE].
- [24] S.L. Zhu, *The Possible interpretations of $Y(4260)$* , *Phys. Lett. B* **625** (2005) 212 [arXiv:hep-ph/0507025] [INSPIRE].
- [25] F.E. Close and P.R. Page, *Gluonic charmonium resonances at BaBar and BELLE?*, *Phys. Lett. B* **628** (2005) 215 [arXiv:hep-ph/0507199] [INSPIRE].
- [26] L. Liu *et al.*, *Excited and exotic charmonium spectroscopy from lattice QCD*, *JHEP* **07** (2012) 126 [arXiv:1204.5425] [INSPIRE].
- [27] E. Braaten *et al.*, *Born-Oppenheimer Approximation for the XYZ Mesons*, *Phys. Rev. D* **90** (2014) 014044 [arXiv:1402.0438] [INSPIRE].
- [28] X. Li and M.B. Voloshin, *$Y(4260)$ and $Y(4360)$ as mixed hadrocharmonium*, *Mod. Phys. Lett. A* **29** (2014) 1450060 [arXiv:1309.1681] [INSPIRE].

- [29] M.B. Voloshin, *Charmonium*, *Prog. Part. Nucl. Phys.* **61** (2008) 455 [arXiv:0711.4556] [INSPIRE].
- [30] F.K. Guo *et al.*, *Evidence that the $Y(4660)$ is an $f_0(980)\psi'$ bound state*, *Phys. Lett. B* **665** (2008) 26 [arXiv:0803.1392] [INSPIRE].
- [31] Z.G. Wang and X.H. Zhang, *Analysis of $Y(4660)$ and related bound states with QCD sum rules*, *Commun. Theor. Phys.* **54** (2010) 323 [arXiv:0905.3784] [INSPIRE].
- [32] Q. Wang *et al.*, *Decoding the riddle of $Y(4260)$ and $Z_c(3900)$* , *Phys. Rev. Lett.* **111** (2013) 132003 [arXiv:1303.6355] [INSPIRE].
- [33] M. Cleven *et al.*, *$Y(4260)$ as the first S -wave open charm vector molecular state?*, *Phys. Rev. D* **90** (2014) 074039 [arXiv:1310.2190] [INSPIRE].
- [34] Q. Wang *et al.*, *$Y(4260)$: hadronic molecule versus hadro-charmonium interpretation*, *Phys. Rev. D* **89** (2014) 034001 [arXiv:1309.4303] [INSPIRE].
- [35] Z.G. Wang, *Analysis of the $Y(4220)$ and $Y(4390)$ as molecular states with QCD sum rules*, *Chin. Phys. C* **41** (2017) 083103 [arXiv:1611.03250] [INSPIRE].
- [36] D.Y. Chen *et al.*, *Nonresonant explanation for the $Y(4260)$ structure observed in the $e^+e^- \rightarrow J\psi\pi^+\pi^-$ process*, *Phys. Rev. D* **83** (2011) 054021 [arXiv:1012.5362] [INSPIRE].
- [37] D.Y. Chen *et al.*, *Unified Fano-like interference picture for charmoniumlike states $Y(4008)$, $Y(4260)$ and $Y(4360)$* , *Phys. Rev. D* **93** (2016) 014011 [arXiv:1512.04157] [INSPIRE].
- [38] A. Martinez Torres *et al.*, *The $Y(4260)$ as a $J/\psi K\bar{K}$ system*, *Phys. Rev. D* **80** (2009) 094012 [arXiv:0906.5333] [INSPIRE].
- [39] X.H. Liu and G. Li, *Exploring the threshold behavior and implications on the nature of $Y(4260)$ and $Z_c(3900)$* , *Phys. Rev. D* **88** (2013) 014013 [arXiv:1306.1384] [INSPIRE].
- [40] C.F. Qiao, *One explanation for the exotic state $Y(4260)$* , *Phys. Lett. B* **639** (2006) 263 [arXiv:hep-ph/0510228] [INSPIRE].
- [41] R. Brandelik *et al.* [DASP Collaboration], *Total Cross-section for Hadron Production by e^+e^- Annihilation at Center-of-mass Energies Between 3.6 and 5.2 GeV*, *Phys. Lett. B* **76** (1978) 361 [INSPIRE].
- [42] M. Ablikim *et al.* [BES Collaboration], *Determination of the $\psi(3770)$, $\psi(4040)$, $\psi(4160)$ and $\psi(4415)$ resonance parameters*, *Phys. Lett. B* **660** (2008) 315 [arXiv:0705.4500] [INSPIRE].
- [43] X.H. Mo *et al.*, *On the leptonic partial widths of the excited ψ states*, *Phys. Rev. D* **82** (2010) 077501 [arXiv:1007.0084] [INSPIRE].
- [44] R. Aaij *et al.* [LHCb Collaboration], *Observation of a resonance in $B^+ \rightarrow K^+\mu^+\mu^-$ decays at low recoil*, *Phys. Rev. Lett.* **111** (2013) 112003 [arXiv:1307.7595] [INSPIRE].
- [45] M. Ablikim *et al.* [BESIII Collaboration], *Measurements of $e^+e^- \rightarrow K_S^0 K^\pm \pi^\mp \pi^0$ and $K_S^0 K^\pm \pi^\mp \eta$ at center-of-mass energies from 3.90 to 4.60 GeV*, *Phys. Rev. D* **99** (2019) 012003 [arXiv:1810.09395] [INSPIRE].
- [46] M. Ablikim *et al.* [BESIII Collaboration], *Precision measurements of $\sigma_B(e^+e^- \rightarrow K_S^0 K^\pm \pi^\mp)$ at center-of-mass energies between 3.8 and 4.6 GeV*, *Phys. Rev. D* **99** (2019) 072005 [arXiv:1808.08733] [INSPIRE].
- [47] M. Ablikim *et al.* [BESIII Collaboration], *Study of $e^+e^- \rightarrow 2(p\bar{p})$ at center-of-mass energies between 4.0 and 4.6 GeV*, *Phys. Rev. D* **103** (2021) 052003 [arXiv:2012.11079] [INSPIRE].

- [48] M. Ablikim *et al.* [BESIII Collaboration], *Cross sections for the reactions $e^+e^- \rightarrow K^+K^-\pi^+\pi^- (\pi^0), K^+K^-K^+K^- (\pi^0), \pi^+\pi^-\pi^+\pi^- (\pi^0), p\bar{p}\pi^+\pi^-\pi^0$ in the energy region between 3.773 and 4.600 GeV*, *Phys. Rev. D* **104** (2021) 112009.
- [49] M. Ablikim *et al.* [BESIII Collaboration], *Search for $Z_c(3900)^\pm \rightarrow \omega\pi^\pm$* , *Phys. Rev. D* **92** (2015) 032009 [arXiv:1507.02068] [INSPIRE].
- [50] M. Ablikim *et al.* [BESIII Collaboration], *Design and Construction of the BESIII Detector*, *Nucl. Instrum. Meth. A* **614** (2010) 345 [arXiv:0911.4960] [INSPIRE].
- [51] C. H. Yu *et al.*, *BEPCII Performance and Beam Dynamics Studies on Luminosity*, *Proceedings of IPAC2016, Busan, Korea, 2016* [INSPIRE].
- [52] K. X. Huang, *et al.*, *Method for detector description transformation to Unity and application in BESIII*, *Nucl. Sci. Tech.* **33**, (2022) 142.
- [53] X. Li *et al.*, *Study of MRPC technology for BESIII endcap-TOF upgrade*, *Radiat. Detect. Technol. Methods* **1** (2017) 13; Y. X. Guo *et al.*, *The study of time calibration for upgraded end cap TOF of BESIII*, *Radiat. Detect. Technol. Methods* **1** (2017) 15; P. Cao *et al.*, *Design and construction of the new BESIII endcap Time-of-Flight system with MRPC Technology*, *Nucl. Instrum. Meth. A* **953** (2020) 163053.
- [54] M. Ablikim *et al.* [BESIII Collaboration], *Measurement of the center-of-mass energies at BESIII via the di-muon process*, *Chin. Phys. C* **40** (2016) 063001 [arXiv:1510.08654] [INSPIRE]; Y.F. Yang *et al.* [BESIII Collaboration], *BAM-00340*; A. Juli and A. Gilman *et al.* [BESIII Collaboration], *BESIII-DOC 580*.
- [55] M. Ablikim *et al.* [BESIII Collaboration], *Precision measurement of the integrated luminosity of the data taken by BESIII at center of mass energies between 3.810 GeV and 4.600 GeV*, *Chin. Phys. C* **39** (2015) 093001 [arXiv:1503.03408] [INSPIRE]; Y.F. Yang *et al.* [BESIII Collaboration], *BAM-00340*.
- [56] Z. Y. Deng *et al.*, *Object-Oriented BESIII Detector Simulation System*, *Chin. Phys. C* **30** (2006) 371.
- [57] S. Agostinelli *et al.*, [GEANT4 Collaboration], *GEANT4—a simulation toolkit*, *Nucl. Instrum. Meth. A* **506** (2003) 250 [INSPIRE].
- [58] Y. T. Liang *et al.*, *A uniform geometry description for simulation, reconstruction and visualization in the BESIII experiment*, *Nucl. Instrum. Meth. A* **603** (2009) 325 [INSPIRE].
- [59] Z. Y. You *et al.*, *A method for detector description exchange among ROOT GEANT4 and GEANT3*, *Chin. Phys. C* **32** (2008) 572.
- [60] S. Jadach *et al.*, *The Precision Monte Carlo event generator KK for two fermion final states in e^+e^- collisions*, *Comput. Phys. Commun.* **130**, 260 (2000) [arXiv:hep-ph/9912214] [INSPIRE]; S. Jadach *et al.*, *Coherent exclusive exponentiation for precision Monte Carlo calculations*, *Phys. Rev. D* **63** (2001) 113009 [arXiv:hep-ph/0006359] [INSPIRE].
- [61] R. G. Ping, *Event generators at BESIII*, *Chin. Phys. C* **32** (2008) 599 [INSPIRE]; D. J. Lange, *The EvtGen particle decay simulation package*, *Nucl. Instr. Meth. A* **462** (2001) 152 [INSPIRE].
- [62] M. Ablikim *et al.* [BESII Collaboration], *Cross section measurements of $e^+e^- \rightarrow \omega\chi_{c0}$ from $\sqrt{s}=4.178$ to 4.278 GeV*, *Phys. Rev. D* **99** (2019) 091103 [arXiv:1903.02359] [INSPIRE].
- [63] R. Aaij *et al.* [LHCb Collaboration], *Observation of $J/\psi p$ Resonances Consistent with*

- Pentaquark States in $\Lambda_b^0 \rightarrow J/\psi K^- p$ Decays*, *Phys. Rev. Lett.* **115** (2015) 072001 [arXiv:1507.03414] [INSPIRE].
- [64] K. Chilikin *et al.* [Belle Collaboration], *Experimental constraints on the spin and parity of the $Z(4430)^+$* , *Phys. Rev. D* **88** (2013) 074026 [arXiv:1306.4894] [INSPIRE].
- [65] H. Chen and R. G. Ping, *Coherent helicity amplitude for sequential decays*, *Phys. Rev. D* **95** (2017) 076010 [arXiv:1704.05184] [INSPIRE].
- [66] S. U. Chung, *A General formulation of covariant helicity coupling amplitudes*, *Phys. Rev. D* **57** (1998) 431 [INSPIRE]; S. U. Chung, *Helicity coupling amplitudes in tensor formalism*, *Phys. Rev. D* **48** (1993) 1225 [INSPIRE]; S. U. Chung and J. M. Friedrich, *Covariant helicity-coupling amplitudes: A New formulation*, *Phys. Rev. D* **78** (2008) 074027 [arXiv:0711.3143] [INSPIRE].
- [67] F. James, *Minuit: A System for Function Minimization and Analysis of the Parameter Errors and Correlations*, *Comput. Phys. Commun.* **10** (1975) 343 [INSPIRE].
- [68] M. Ablikim *et al.* [BESII Collaboration], *The sigma pole in $J/\psi \rightarrow \omega \pi^+ \pi^-$* , *Phys. Lett. B* **598** (2004) 149 [arXiv:hep-ex/0406038] [INSPIRE].
- [69] M. Ablikim *et al.* [BESII Collaboration], *Production of sigma in $\psi(2S) \rightarrow \pi^+ \pi^- J/\psi$* , *Phys. Lett. B* **645** (2007) 19 [arXiv:hep-ex/0610023] [INSPIRE].
- [70] V. P. Druzhinin, S. I. Eidelman, S. I. Serednyakov, and E. P. Solodov, *Hadron production via e^+e^- collisions with initial state radiation*, *Rev. Mod. Phys.* **83** (2011) 1545 [arXiv:hep-ph/1105.4975] [INSPIRE].
- [71] E. A. Kuraev, and V. S. Fadin, *On Radiative Corrections to e^+e^- Single Photon Annihilation at High-Energy*, *Sov. J. Nucl. Phys.* **41** (1985) 466-472 [INSPIRE].
- [72] R. G. Ping *et al.*, *Tuning and validation of hadronic event generator for R value measurements in the tau-charm region*, *Chinese Phys. C* **40** (2016) 113002
- [73] S. Eidelman and F. Jegerlehner, *Hadronic contributions to $(g-2)$ of the leptons and to the effective fine structure constant $\alpha(M_Z^2)$* , *Z. Phys. C* **67** (1995) 585 [arXiv:hep-ph/9502298] [INSPIRE].
- [74] F. Jegerlehner, *Precision measurements of $\sigma_{hadronic}$ for $\alpha_{eff}(E)$ at ILC energies and $(g-2)_\mu$* , *Nucl. Phys. B* **162** (2006) 22 [arXiv:hep-ph/0608329] [INSPIRE].
- [75] F. Jegerlehner, *The Running fine structure constant α_E via the Adler function*, *Nucl. Phys. B Proc. Suppl.* **181** (2008) 135 [arXiv:0807.4206] [INSPIRE].
- [76] F. Jegerlehner, *Theoretical precision in estimates of the hadronic contributions to $(g-2)_\mu$ and $\alpha_{QED}(M_Z)$* , *Nucl. Phys. B Proc. Suppl.* **126** (2004) 325 [arXiv:hep-ph/0310234] [INSPIRE].
- [77] F. Jegerlehner, *Hadronic vacuum polarization effects in $\alpha_{em}(M_Z)$* , *Mini-Workshop on Electroweak Precision Data and the Higgs Mass, (2003) 97* [arXiv:hep-ph/0308117] [INSPIRE].
- [78] B. Aubert *et al.* [Babar Collaboration], *The $e^+e^- \rightarrow 2(\pi^+\pi^-)\pi^0, 2(\pi^+\pi^-)\eta, K^+K^-\pi^+\pi^-\pi^0$ and $K^+K^-\pi^+\pi^-\eta$ Cross Sections Measured with Initial-State Radiation*, *Phys. Rev. D* **76** (2007) 092005 [arXiv:0708.2461] [INSPIRE].
- [79] M. Ablikim *et al.* [BESIII Collaboration], *Measurements of the branching fractions of*

$\eta_c \rightarrow K^+ K^- \pi^0, K_S^0 K^\pm \pi^\mp, 2(\pi^+ \pi^- \pi^0)$ and $p\bar{p}$, *Phys. Rev. D* **100** (2019) 012003 [[arXiv:1903.05375](#)] [[INSPIRE](#)].

- [80] M. Ablikim *et al.* [BESIII Collaboration], *Search for hadronic transition $\chi_{cJ} \rightarrow \eta_c \pi^+ \pi^-$ and observation of $\chi_{cJ} \rightarrow K \bar{K} \pi \pi$* , *Phys. Rev. D* **87** (2013) 012002 [[arXiv:1208.4805](#)] [[INSPIRE](#)].
- [81] B. P. Roe, *Probability and Statistics in Experimental Physics, 2nd edn., New York (2001)*.
- [82] X. H. Mo, Unbiased χ^2 Estimator for Linear Function Fit Involving Correlated Data, *HEPNP* **31** (2007) 745.

M. Ablikim¹, M. N. Achasov^{11,b}, P. Adlarson⁷⁰, M. Albrecht⁴, R. Aliberti³¹, A. Amoroso^{69A,69C},
M. R. An³⁵, Q. An^{66,53}, Y. Bai⁵², O. Bakina³², R. Baldini Ferroli^{26A}, I. Balossino^{27A}, Y. Ban^{42,g},
V. Batozskaya^{1,40}, D. Becker³¹, K. Begzsuren²⁹, N. Berger³¹, M. Bertani^{26A}, D. Bettoni^{27A},
F. Bianchi^{69A,69C}, E. Bianco^{69A,69C}, J. Bloms⁶³, A. Bortone^{69A,69C}, I. Boyko³², R. A. Briere⁵,
A. Brueggemann⁶³, H. Cai⁷¹, X. Cai^{1,53}, A. Calcaterra^{26A}, G. F. Cao^{1,58}, N. Cao^{1,58},
S. A. Cetin^{57A}, J. F. Chang^{1,53}, W. L. Chang^{1,58}, G. R. Che³⁹, G. Chelkov^{32,a}, C. Chen³⁹,
Chao Chen⁵⁰, G. Chen¹, H. S. Chen^{1,58}, M. L. Chen^{1,53}, S. J. Chen³⁸, S. M. Chen⁵⁶, T. Chen¹,
X. R. Chen^{28,58}, X. T. Chen¹, Y. B. Chen^{1,53}, Z. J. Chen^{23,h}, W. S. Cheng^{69C}, S. K. Choi⁵⁰,
X. Chu³⁹, G. Cibinetto^{27A}, F. Cossio^{69C}, J. J. Cui⁴⁵, H. L. Dai^{1,53}, J. P. Dai⁷³, A. Dbeyssi¹⁷,
R. E. de Boer⁴, D. Dedovich³², Z. Y. Deng¹, A. Denig³¹, I. Denysenko³², M. Destefanis^{69A,69C},
F. De Mori^{69A,69C}, Y. Ding³⁰, Y. Ding³⁶, J. Dong^{1,53}, L. Y. Dong^{1,58}, M. Y. Dong^{1,53,58},
X. Dong⁷¹, S. X. Du⁷⁵, Z. H. Duan³⁸, P. Egorov^{32,a}, Y. L. Fan⁷¹, J. Fang^{1,53}, S. S. Fang^{1,58},
W. X. Fang¹, Y. Fang¹, R. Farinelli^{27A}, L. Fava^{69B,69C}, F. Feldbauer⁴, G. Felici^{26A},
C. Q. Feng^{66,53}, J. H. Feng⁵⁴, K. Fischer⁶⁴, M. Fritsch⁴, C. Fritsch⁶³, C. D. Fu¹, H. Gao⁵⁸,
Y. N. Gao^{42,g}, Yang Gao^{66,53}, S. Garbolino^{69C}, I. Garzia^{27A,27B}, P. T. Ge⁷¹, Z. W. Ge³⁸,
C. Geng⁵⁴, E. M. Gersabeck⁶², A. Gilman⁶⁴, K. Goetzen¹², L. Gong³⁶, W. X. Gong^{1,53},
W. Gradl³¹, M. Greco^{69A,69C}, L. M. Gu³⁸, M. H. Gu^{1,53}, Y. T. Gu¹⁴, C. Y. Guan^{1,58},
A. Q. Guo^{28,58}, L. B. Guo³⁷, R. P. Guo⁴⁴, Y. P. Guo^{10,f}, A. Guskov^{32,a}, W. Y. Han³⁵,
X. Q. Hao¹⁸, F. A. Harris⁶⁰, K. K. He⁵⁰, K. L. He^{1,58}, F. H. Heinsius⁴, C. H. Heinz³¹,
Y. K. Heng^{1,53,58}, C. Herold⁵⁵, G. Y. Hou^{1,58}, Y. R. Hou⁵⁸, Z. L. Hou¹, H. M. Hu^{1,58}, J. F. Hu^{51,i},
T. Hu^{1,53,58}, Y. Hu¹, G. S. Huang^{66,53}, K. X. Huang⁵⁴, L. Q. Huang^{28,58}, X. T. Huang⁴⁵,
Y. P. Huang¹, Z. Huang^{42,g}, T. Hussain⁶⁸, N. Hüsken^{25,31}, W. Imoehl²⁵, M. Irshad^{66,53},
J. Jackson²⁵, S. Jaeger⁴, S. Janchiv²⁹, E. Jang⁵⁰, J. H. Jeong⁵⁰, Q. Ji¹, Q. P. Ji¹⁸, X. B. Ji^{1,58},
X. L. Ji^{1,53}, Y. Y. Ji⁴⁵, Z. K. Jia^{66,53}, S. S. Jiang³⁵, X. S. Jiang^{1,53,58}, Y. Jiang⁵⁸, J. B. Jiao⁴⁵,
Z. Jiao²¹, S. Jin³⁸, Y. Jin⁶¹, M. Q. Jing^{1,58}, T. Johansson⁷⁰, N. Kalantar-Nayestanaki⁵⁹,
X. S. Kang³⁶, R. Kappert⁵⁹, M. Kavatsyuk⁵⁹, B. C. Ke⁷⁵, I. K. Keshk⁴, A. Khoukaz⁶³, R. Kiuchi¹,
R. Kliemt¹², L. Koch³³, O. B. Kolcu^{57A}, B. Kopf⁴, M. Kuemmel⁴, M. Kuessner⁴, A. Kupsc^{40,70},
W. Kühn³³, J. J. Lane⁶², J. S. Lange³³, P. Larin¹⁷, A. Lavania²⁴, L. Lavezzi^{69A,69C},
Z. H. Lei^{66,53}, H. Leithoff³¹, M. Lellmann³¹, T. Lenz³¹, C. Li³⁹, C. Li⁴³, C. H. Li³⁵, Cheng Li^{66,53},
D. M. Li⁷⁵, F. Li^{1,53}, G. Li¹, H. Li^{66,53}, H. Li⁴⁷, H. B. Li^{1,58}, H. J. Li¹⁸, H. N. Li^{51,i}, J. Q. Li⁴,
J. S. Li⁵⁴, J. W. Li⁴⁵, Ke Li¹, L. J Li¹, L. K. Li¹, Lei Li³, M. H. Li³⁹, P. R. Li^{34,j,k}, S. X. Li¹⁰,
S. Y. Li⁵⁶, T. Li⁴⁵, W. D. Li^{1,58}, W. G. Li¹, X. H. Li^{66,53}, X. L. Li⁴⁵, Xiaoyu Li^{1,58}, Y. G. Li^{42,g},
Z. X. Li¹⁴, Z. Y. Li⁵⁴, C. Liang³⁸, H. Liang³⁰, H. Liang^{1,58}, H. Liang^{66,53}, Y. F. Liang⁴⁹,
Y. T. Liang^{28,58}, G. R. Liao¹³, L. Z. Liao⁴⁵, J. Libby²⁴, A. Limphirat⁵⁵, C. X. Lin⁵⁴,
D. X. Lin^{28,58}, T. Lin¹, B. J. Liu¹, C. Liu³⁰, C. X. Liu¹, D. Liu^{17,66}, F. H. Liu⁴⁸, Fang Liu¹,
Feng Liu⁶, G. M. Liu^{51,i}, H. Liu^{34,j,k}, H. B. Liu¹⁴, H. M. Liu^{1,58}, Huanhuan Liu¹, Huihui Liu¹⁹,
J. B. Liu^{66,53}, J. L. Liu⁶⁷, J. Y. Liu^{1,58}, K. Liu¹, K. Y. Liu³⁶, Ke Liu²⁰, L. Liu^{66,53}, Lu Liu³⁹,
M. H. Liu^{10,f}, P. L. Liu¹, Q. Liu⁵⁸, S. B. Liu^{66,53}, T. Liu^{10,f}, W. K. Liu³⁹, W. M. Liu^{66,53},
X. Liu^{34,j,k}, Y. Liu^{34,j,k}, Y. B. Liu³⁹, Z. A. Liu^{1,53,58}, Z. Q. Liu⁴⁵, X. C. Lou^{1,53,58}, F. X. Lu⁵⁴,
H. J. Lu²¹, J. G. Lu^{1,53}, X. L. Lu¹, Y. Lu⁷, Y. P. Lu^{1,53}, Z. H. Lu¹, C. L. Luo³⁷, M. X. Luo⁷⁴,
T. Luo^{10,f}, X. L. Luo^{1,53}, X. R. Lyu⁵⁸, Y. F. Lyu³⁹, F. C. Ma³⁶, H. L. Ma¹, L. L. Ma⁴⁵,
M. M. Ma^{1,58}, Q. M. Ma¹, R. Q. Ma^{1,58}, R. T. Ma⁵⁸, X. Y. Ma^{1,53}, Y. Ma^{42,g}, F. E. Maas¹⁷,
M. Maggiora^{69A,69C}, S. Maldaner⁴, S. Malde⁶⁴, Q. A. Malik⁶⁸, A. Mangoni^{26B}, Y. J. Mao^{42,g},
Z. P. Mao¹, S. Marcello^{69A,69C}, Z. X. Meng⁶¹, J. G. Messchendorp^{12,59}, G. Mezzadri^{27A},
H. Miao¹, T. J. Min³⁸, R. E. Mitchell²⁵, X. H. Mo^{1,53,58}, N. Yu. Muchnoi^{11,b}, Y. Nefedov³²,
F. Nerling^{17,d}, I. B. Nikolaev^{11,b}, Z. Ning^{1,53}, S. Nisar^{9,l}, Y. Niu⁴⁵, S. L. Olsen⁵⁸,
Q. Ouyang^{1,53,58}, S. Pacetti^{26B,26C}, X. Pan^{10,f}, Y. Pan⁵², A. Pathak³⁰, M. Pelizaeus⁴,
H. P. Peng^{66,53}, K. Peters^{12,d}, J. L. Ping³⁷, R. G. Ping^{1,58}, S. Plura³¹, S. Pogodin³²,

V. Prasad^{66,53}, F. Z. Qi¹, H. Qi^{66,53}, H. R. Qi⁵⁶, M. Qi³⁸, T. Y. Qi^{10,f}, S. Qian^{1,53}, W. B. Qian⁵⁸,
Z. Qian⁵⁴, C. F. Qiao⁵⁸, J. J. Qin⁶⁷, L. Q. Qin¹³, X. P. Qin^{10,f}, X. S. Qin⁴⁵, Z. H. Qin^{1,53},
J. F. Qiu¹, S. Q. Qu⁵⁶, K. H. Rashid⁶⁸, C. F. Redmer³¹, K. J. Ren³⁵, A. Rivetti^{69C}, V. Rodin⁵⁹,
M. Rolo^{69C}, G. Rong^{1,58}, Ch. Rosner¹⁷, S. N. Ruan³⁹, A. Sarantsev^{32,c}, Y. Schelhaas³¹,
C. Schnier⁴, K. Schoenning⁷⁰, M. Scodreggio^{27A,27B}, K. Y. Shan^{10,f}, W. Shan²², X. Y. Shan^{66,53},
J. F. Shangguan⁵⁰, L. G. Shao^{1,58}, M. Shao^{66,53}, C. P. Shen^{10,f}, H. F. Shen^{1,58}, X. Y. Shen^{1,58},
B. A. Shi⁵⁸, H. C. Shi^{66,53}, J. Y. Shi¹, Q. Q. Shi⁵⁰, R. S. Shi^{1,58}, X. Shi^{1,53}, X. D Shi^{66,53},
J. J. Song¹⁸, W. M. Song^{30,1}, Y. X. Song^{42,g}, S. Sosio^{69A,69C}, S. Spataro^{69A,69C}, F. Stieler³¹,
K. X. Su⁷¹, P. P. Su⁵⁰, Y. J. Su⁵⁸, G. X. Sun¹, H. Sun⁵⁸, H. K. Sun¹, J. F. Sun¹⁸, L. Sun⁷¹,
S. S. Sun^{1,58}, T. Sun^{1,58}, W. Y. Sun³⁰, Y. J. Sun^{66,53}, Y. Z. Sun¹, Z. T. Sun⁴⁵, Y. H. Tan⁷¹,
Y. X. Tan^{66,53}, C. J. Tang⁴⁹, G. Y. Tang¹, J. Tang⁵⁴, L. Y. Tao⁶⁷, Q. T. Tao^{23,h}, M. Tat⁶⁴,
J. X. Teng^{66,53}, V. Thoren⁷⁰, W. H. Tian⁴⁷, Y. Tian^{28,58}, I. Uman^{57B}, B. Wang¹, B. L. Wang⁵⁸,
C. W. Wang³⁸, D. Y. Wang^{42,g}, F. Wang⁶⁷, H. J. Wang^{34,j,k}, H. P. Wang^{1,58}, K. Wang^{1,53},
L. L. Wang¹, M. Wang⁴⁵, M. Z. Wang^{42,g}, Meng Wang^{1,58}, S. Wang^{10,f}, S. Wang¹³, T. Wang^{10,f},
T. J. Wang³⁹, W. Wang⁵⁴, W. H. Wang⁷¹, W. P. Wang^{66,53}, X. Wang^{42,g}, X. F. Wang^{34,j,k},
X. L. Wang^{10,f}, Y. Wang⁵⁶, Y. D. Wang⁴¹, Y. F. Wang^{1,53,58}, Y. H. Wang⁴³, Y. Q. Wang¹,
Yaqian Wang^{16,1}, Z. Wang^{1,53}, Z. Y. Wang^{1,58}, Ziyi Wang⁵⁸, D. H. Wei¹³, F. Weidner⁶³,
S. P. Wen¹, D. J. White⁶², U. Wiedner⁴, G. Wilkinson⁶⁴, M. Wolke⁷⁰, L. Wollenberg⁴,
J. F. Wu^{1,58}, L. H. Wu¹, L. J. Wu^{1,58}, X. Wu^{10,f}, X. H. Wu³⁰, Y. Wu⁶⁶, Y. J. Wu²⁸, Z. Wu^{1,53},
L. Xia^{66,53}, T. Xiang^{42,g}, D. Xiao^{34,j,k}, G. Y. Xiao³⁸, H. Xiao^{10,f}, S. Y. Xiao¹, Y. L. Xiao^{10,f},
Z. J. Xiao³⁷, C. Xie³⁸, X. H. Xie^{42,g}, Y. Xie⁴⁵, Y. G. Xie^{1,53}, Y. H. Xie⁶, Z. P. Xie^{66,53},
T. Y. Xing^{1,58}, C. F. Xu¹, C. J. Xu⁵⁴, G. F. Xu¹, H. Y. Xu⁶¹, Q. J. Xu¹⁵, X. P. Xu⁵⁰, Y. C. Xu⁵⁸,
Z. P. Xu³⁸, F. Yan^{10,f}, L. Yan^{10,f}, W. B. Yan^{66,53}, W. C. Yan⁷⁵, H. J. Yang^{46,e}, H. L. Yang³⁰,
H. X. Yang¹, L. Yang⁴⁷, Tao Yang¹, Y. F. Yang³⁹, Y. X. Yang^{1,58}, Yifan Yang^{1,58}, M. Ye^{1,53},
M. H. Ye⁸, J. H. Yin¹, Z. Y. You⁵⁴, B. X. Yu^{1,53,58}, C. X. Yu³⁹, G. Yu^{1,58}, T. Yu⁶⁷, X. D. Yu^{42,g},
C. Z. Yuan^{1,58}, L. Yuan², S. C. Yuan¹, X. Q. Yuan¹, Y. Yuan^{1,58}, Z. Y. Yuan⁵⁴, C. X. Yue³⁵,
A. A. Zafar⁶⁸, F. R. Zeng⁴⁵, X. Zeng⁶, Y. Zeng^{23,h}, X. Y. Zhai³⁰, Y. H. Zhan⁵⁴, A. Q. Zhang¹,
B. L. Zhang¹, B. X. Zhang¹, D. H. Zhang³⁹, G. Y. Zhang¹⁸, H. Zhang⁶⁶, H. H. Zhang⁵⁴,
H. H. Zhang³⁰, H. Y. Zhang^{1,53}, J. L. Zhang⁷², J. Q. Zhang³⁷, J. W. Zhang^{1,53,58},
J. X. Zhang^{34,j,k}, J. Y. Zhang¹, J. Z. Zhang^{1,58}, Jianyu Zhang^{1,58}, Jiawei Zhang^{1,58},
L. M. Zhang⁵⁶, L. Q. Zhang⁵⁴, Lei Zhang³⁸, P. Zhang¹, Q. Y. Zhang^{35,75}, Shuihan Zhang^{1,58},
Shulei Zhang^{23,h}, X. D. Zhang⁴¹, X. M. Zhang¹, X. Y. Zhang⁴⁵, X. Y. Zhang⁵⁰, Y. Zhang⁶⁴, Y.
T. Zhang⁷⁵, Y. H. Zhang^{1,53}, Yan Zhang^{66,53}, Yao Zhang¹, Z. H. Zhang¹, Z. L. Zhang³⁰,
Z. Y. Zhang³⁹, Z. Y. Zhang⁷¹, G. Zhao¹, J. Zhao³⁵, J. Y. Zhao^{1,58}, J. Z. Zhao^{1,53}, Lei Zhao^{66,53},
Ling Zhao¹, M. G. Zhao³⁹, S. J. Zhao⁷⁵, Y. B. Zhao^{1,53}, Y. X. Zhao^{28,58}, Z. G. Zhao^{66,53},
A. Zhemchugov^{32,a}, B. Zheng⁶⁷, J. P. Zheng^{1,53}, Y. H. Zheng⁵⁸, B. Zhong³⁷, C. Zhong⁶⁷,
X. Zhong⁵⁴, H. Zhou⁴⁵, L. P. Zhou^{1,58}, X. Zhou⁷¹, X. K. Zhou⁵⁸, X. R. Zhou^{66,53}, X. Y. Zhou³⁵,
Y. Z. Zhou^{10,f}, J. Zhu³⁹, K. Zhu¹, K. J. Zhu^{1,53,58}, L. X. Zhu⁵⁸, S. H. Zhu⁶⁵, S. Q. Zhu³⁸,
T. J. Zhu⁷², W. J. Zhu^{10,f}, Y. C. Zhu^{66,53}, Z. A. Zhu^{1,58}, J. H. Zou¹

(BESIII Collaboration)

¹ *Institute of High Energy Physics, Beijing 100049, People's Republic of China*

² *Beihang University, Beijing 100191, People's Republic of China*

³ *Beijing Institute of Petrochemical Technology, Beijing 102617, People's Republic of China*

⁴ *Bochum Ruhr-University, D-44780 Bochum, Germany*

⁵ *Carnegie Mellon University, Pittsburgh, Pennsylvania 15213, USA*

⁶ *Central China Normal University, Wuhan 430079, People's Republic of China*

⁷ *Central South University, Changsha 410083, People's Republic of China*

- ⁸ *China Center of Advanced Science and Technology, Beijing 100190, People's Republic of China*
- ⁹ *COMSATS University Islamabad, Lahore Campus, Defence Road, Off Raiwind Road, 54000 Lahore, Pakistan*
- ¹⁰ *Fudan University, Shanghai 200433, People's Republic of China*
- ¹¹ *G.I. Budker Institute of Nuclear Physics SB RAS (BINP), Novosibirsk 630090, Russia*
- ¹² *GSI Helmholtzcentre for Heavy Ion Research GmbH, D-64291 Darmstadt, Germany*
- ¹³ *Guangxi Normal University, Guilin 541004, People's Republic of China*
- ¹⁴ *Guangxi University, Nanning 530004, People's Republic of China*
- ¹⁵ *Hangzhou Normal University, Hangzhou 310036, People's Republic of China*
- ¹⁶ *Hebei University, Baoding 071002, People's Republic of China*
- ¹⁷ *Helmholtz Institute Mainz, Staudinger Weg 18, D-55099 Mainz, Germany*
- ¹⁸ *Henan Normal University, Xinxiang 453007, People's Republic of China*
- ¹⁹ *Henan University of Science and Technology, Luoyang 471003, People's Republic of China*
- ²⁰ *Henan University of Technology, Zhengzhou 450001, People's Republic of China*
- ²¹ *Huangshan College, Huangshan 245000, People's Republic of China*
- ²² *Hunan Normal University, Changsha 410081, People's Republic of China*
- ²³ *Hunan University, Changsha 410082, People's Republic of China*
- ²⁴ *Indian Institute of Technology Madras, Chennai 600036, India*
- ²⁵ *Indiana University, Bloomington, Indiana 47405, USA*
- ²⁶ *INFN Laboratori Nazionali di Frascati , (A)INFN Laboratori Nazionali di Frascati, I-00044, Frascati, Italy; (B)INFN Sezione di Perugia, I-06100, Perugia, Italy; (C)University of Perugia, I-06100, Perugia, Italy*
- ²⁷ *INFN Sezione di Ferrara, (A)INFN Sezione di Ferrara, I-44122, Ferrara, Italy; (B)University of Ferrara, I-44122, Ferrara, Italy*
- ²⁸ *Institute of Modern Physics, Lanzhou 730000, People's Republic of China*
- ²⁹ *Institute of Physics and Technology, Peace Avenue 54B, Ulaanbaatar 13330, Mongolia*
- ³⁰ *Jilin University, Changchun 130012, People's Republic of China*
- ³¹ *Johannes Gutenberg University of Mainz, Johann-Joachim-Becher-Weg 45, D-55099 Mainz, Germany*
- ³² *Joint Institute for Nuclear Research, 141980 Dubna, Moscow region, Russia*
- ³³ *Justus-Liebig-Universitaet Giessen, II. Physikalisches Institut, Heinrich-Buff-Ring 16, D-35392 Giessen, Germany*
- ³⁴ *Lanzhou University, Lanzhou 730000, People's Republic of China*
- ³⁵ *Liaoning Normal University, Dalian 116029, People's Republic of China*
- ³⁶ *Liaoning University, Shenyang 110036, People's Republic of China*
- ³⁷ *Nanjing Normal University, Nanjing 210023, People's Republic of China*
- ³⁸ *Nanjing University, Nanjing 210093, People's Republic of China*
- ³⁹ *Nankai University, Tianjin 300071, People's Republic of China*
- ⁴⁰ *National Centre for Nuclear Research, Warsaw 02-093, Poland*
- ⁴¹ *North China Electric Power University, Beijing 102206, People's Republic of China*
- ⁴² *Peking University, Beijing 100871, People's Republic of China*
- ⁴³ *Qufu Normal University, Qufu 273165, People's Republic of China*
- ⁴⁴ *Shandong Normal University, Jinan 250014, People's Republic of China*
- ⁴⁵ *Shandong University, Jinan 250100, People's Republic of China*
- ⁴⁶ *Shanghai Jiao Tong University, Shanghai 200240, People's Republic of China*
- ⁴⁷ *Shanxi Normal University, Linfen 041004, People's Republic of China*
- ⁴⁸ *Shanxi University, Taiyuan 030006, People's Republic of China*
- ⁴⁹ *Sichuan University, Chengdu 610064, People's Republic of China*

- ⁵⁰ *Soochow University, Suzhou 215006, People's Republic of China*
- ⁵¹ *South China Normal University, Guangzhou 510006, People's Republic of China*
- ⁵² *Southeast University, Nanjing 211100, People's Republic of China*
- ⁵³ *State Key Laboratory of Particle Detection and Electronics, Beijing 100049, Hefei 230026, People's Republic of China*
- ⁵⁴ *Sun Yat-Sen University, Guangzhou 510275, People's Republic of China*
- ⁵⁵ *Suranaree University of Technology, University Avenue 111, Nakhon Ratchasima 30000, Thailand*
- ⁵⁶ *Tsinghua University, Beijing 100084, People's Republic of China*
- ⁵⁷ *Turkish Accelerator Center Particle Factory Group, (A)Istinye University, 34010, Istanbul, Turkey; (B)Near East University, Nicosia, North Cyprus, Mersin 10, Turkey*
- ⁵⁸ *University of Chinese Academy of Sciences, Beijing 100049, People's Republic of China*
- ⁵⁹ *University of Groningen, NL-9747 AA Groningen, The Netherlands*
- ⁶⁰ *University of Hawaii, Honolulu, Hawaii 96822, USA*
- ⁶¹ *University of Jinan, Jinan 250022, People's Republic of China*
- ⁶² *University of Manchester, Oxford Road, Manchester, M13 9PL, United Kingdom*
- ⁶³ *University of Muenster, Wilhelm-Klemm-Strasse 9, 48149 Muenster, Germany*
- ⁶⁴ *University of Oxford, Keble Road, Oxford OX13RH, United Kingdom*
- ⁶⁵ *University of Science and Technology Liaoning, Anshan 114051, People's Republic of China*
- ⁶⁶ *University of Science and Technology of China, Hefei 230026, People's Republic of China*
- ⁶⁷ *University of South China, Hengyang 421001, People's Republic of China*
- ⁶⁸ *University of the Punjab, Lahore-54590, Pakistan*
- ⁶⁹ *University of Turin and INFN, (A)University of Turin, I-10125, Turin, Italy; (B)University of Eastern Piedmont, I-15121, Alessandria, Italy; (C)INFN, I-10125, Turin, Italy*
- ⁷⁰ *Uppsala University, Box 516, SE-75120 Uppsala, Sweden*
- ⁷¹ *Wuhan University, Wuhan 430072, People's Republic of China*
- ⁷² *Xinyang Normal University, Xinyang 464000, People's Republic of China*
- ⁷³ *Yunnan University, Kunming 650500, People's Republic of China*
- ⁷⁴ *Zhejiang University, Hangzhou 310027, People's Republic of China*
- ⁷⁵ *Zhengzhou University, Zhengzhou 450001, People's Republic of China*
- ^a *Also at the Moscow Institute of Physics and Technology, Moscow 141700, Russia*
- ^b *Also at the Novosibirsk State University, Novosibirsk, 630090, Russia*
- ^c *Also at the NRC "Kurchatov Institute", PNPI, 188300, Gatchina, Russia*
- ^d *Also at Goethe University Frankfurt, 60323 Frankfurt am Main, Germany*
- ^e *Also at Key Laboratory for Particle Physics, Astrophysics and Cosmology, Ministry of Education; Shanghai Key Laboratory for Particle Physics and Cosmology; Institute of Nuclear and Particle Physics, Shanghai 200240, People's Republic of China*
- ^f *Also at Key Laboratory of Nuclear Physics and Ion-beam Application (MOE) and Institute of Modern Physics, Fudan University, Shanghai 200443, People's Republic of China*
- ^g *Also at State Key Laboratory of Nuclear Physics and Technology, Peking University, Beijing 100871, People's Republic of China*
- ^h *Also at School of Physics and Electronics, Hunan University, Changsha 410082, China*
- ⁱ *Also at Guangdong Provincial Key Laboratory of Nuclear Science, Institute of Quantum Matter, South China Normal University, Guangzhou 510006, China*
- ^j *Also at Frontiers Science Center for Rare Isotopes, Lanzhou University, Lanzhou 730000, People's Republic of China*
- ^k *Also at Lanzhou Center for Theoretical Physics, Lanzhou University, Lanzhou 730000, People's Republic of China*

^l Also at the Department of Mathematical Sciences, IBA, Karachi , Pakistan